Impedance Modulation Control of a Lower Limb Exoskeleton to Assist Sit-to-Stand Movements

Weiguang Huo, Huiseok Moon, Mohamed A. Alouane, Vincent Bonnet, Jian Huang, Yacine Amirat, Ravi Vaidyanathan, and Samer Mohammed

***Abstract*—As an important movement of the daily living activities, sit-to-stand (STS) movement is usually a difficult task facing elderly and dependent people. In this article, a novel impedance modulation strategy of a lower limb exoskeleton is proposed to provide appropriate power and balance assistance during STS movements while preserving the wearer's control priority. The impedance modulation control strategy ensures adaptation of the mechanical impedance of the human-exoskeleton system towards a desired one requiring less wearer's effect while reinforcing the wearer's balance control ability during STS movements. A human joint torque observer is designed to estimate the joint torques developed by the wearer using joint position kinematics instead of electromyography (EMG) or force sensors; a time-varying desired impedance model is proposed according to the wearer's lower limb motion ability. A virtual environmental force is designed for the balance reinforcement control. Stability and robustness of the proposed method are theoretically analyzed. Simulations were implemented to illustrate the characteristics and performance of the proposed approach. Experiments with four healthy subjects were carried out to evaluate the effectiveness of the proposed method and show satisfactory results in terms of appropriate power assist and balance reinforcement.**

***Index Terms*—Sit-to-stand movement, exoskeleton, impedance control, balance reinforcement.**

I. Introduction

SIT-to-stand (STS), the capacity to rise from a chair to a standing position without loss of balance, is a fundamental prerequisite to almost all simple ambulatory activities of daily living (ADLs). It is far more demanding than movements such as walking, in particular as the body ages [1]. STS demands a complex skill set involving synchronization of trunk and lower limb movement, muscle strength, and control of centre of mass (CoM) for equilibrium and stability [2]. It requires whole body movements, large joint torques and high core strength. Difficulty in STS is a massive issue clinically for a large segment of the population, severely impacting autonomy of this population and increasing risk of fall injuries. Groups at high risk include the elderly, patients suffering from musculoskeletal disorders, arthritis, or neurological conditions such as stroke or Parkinson's Disease. Factors that impact STS movement, or result in failed STS (e.g., "sitback" and "step") include balance control, coordination impairment, and lower limb muscle weakness [3]. In particular, age-related changes in muscle and joint forces have been demonstrated during STS [4] and performing STS demands up to 97% of available muscle strength in the elderly [5]. Stroke patients have also been shown to take significantly longer to execute simple STS movements, entailing greater risk of falls and poorer capacity to function [6]. Beyond direct risks of injury and functional impairment, compensation in upper limb muscles and joints in patients with difficulty in STS augments lower limb atrophy and declines remaining body strength, "leading to increased vulnerability, dependence, and risk of institutionalisation" [4]. The importance of STS for mobility and its role in increased risk of social isolation have led to a range of rehabilitation therapies in practice [7]; however, challenges remain to exploit the further potential for assistive technology for clinical use in this arena.

Research on powered lower limb exoskeletons to assist individuals suffering from neurological injuries and/or muscular weakness during daily-life activities has proliferated in recent years [8]–[10], yet the complex dynamics of human-centered STS has not been fully addressed, much less resolved or translated clinically today [10]. Assistive strategies for STS movements can be broadly divided into two main categories, based on the patient's conditions: 1) patients generating zero or negligible lower limb muscular force (e.g. patients with complete spinal cord injury or severe muscle atrophy) for whom the exoskeleton must provide all required torques (e.g., [11]–[13]); and 2) patients with the capacity to provide partial muscular efforts (e.g. elderly or stroke patients), for whom the exoskeleton complements the wearers' strength to complete a successful STS movement (e.g., [14]–[16]). Motivation for the first category principally lies in increased functionality for immobile patients where the exoskeleton is used to generate more power without requiring coordination with lower limb muscle movements. Need for the second category lies in the combination of augmenting mobility, lowering risk of injury and, potentially, supporting rehabilitation. In this case, the exoskeleton must coordinate its activity with wearer's muscle action. The majority of the elderly with difficulty in STS show serious risk of falls from loss of control [3] and sustained damage due to compensation [4]. However, patients under the second condition also have the potential of rehabilitation if exoskeleton control can synergise action with muscle activity. In this investigation, we focus on the second category of assistive strategies. Specifically, we introduce an architecture for STS movement support using a powered exoskeleton for wearers suffering from partial impairment of lower limb

W. Huo and R. Vaidyanathan are with the Department of Mechanical Engineering and DRI-CRT, Imperial College London, London, UK. e-mail: {w.huo, r.vaidyanathan}@imperial.ac.uk

H. Moon, M. A. Alouane,V. Bonnet, Y. Amirat and S. Mohammed are with Univ Paris Est Créteil, LISSI, F-94400 Vitry, France.

J. Huang is with the School of Automation, Huazhong University of Science and Technology, Wuhan 430074, China.

muscular capacity.

An intuitive method for the control of exoskeletons assisting STS movements is to track a pre-designed reference such as joint position [11], [12], [17] and joint velocity [16]. Such methods are popularly used to assist individuals with complete paraplegia. Meanwhile, balance control is essential for those patients, in which the wearer's CoM is generally used to assess the STS balance and guide the design of the reference trajectory, e.g., [12], [17]. The primary purpose of these methods is to assist the wearer to accomplish a successful STS movement without considering the wearer's voluntary capabilities. Therefore, reference tracking based algorithms largely ignore the control ability of the wearer with partial motor ability to achieve STS movements.

To effectively assist individuals with partial motor ability, an important control challenge for lower limb exoskeletons assisting STS movements lies in the ability to estimate the wearer's motion intention in real-time. In this perspective, different approaches have been developed in the literature, ranging from phase-based algorithms to multisensory-based sophisticated ones [18], [14], [19], [20]. A common method is to divide the STS movement into several sub-phases, and then, detect the transitions between the phases using threshold-based methods [21] or machine-learning-based algorithms [18], [22]. Reference-based impedance/admittance control methods are, however, still employed for each phase, e.g., [18], [21]. To obtain a continuous estimation of the wearer's motion intention, the joint torque generated by the wearer is generally used as a representative metric [14], [23]. Estimation of human joint torques is commonly done using electromyography (EMG) [14], [19] and force/torque sensors [20]. However, the two aforementioned methods face some limitations when used in the context of daily living activities. EMG sensors are usually sensitive to many factors, such as electrodes placement and neighbouring muscles signals, which result in a cumbersome one-use calibration for ensuring an accurate EMG-based model. Torque/force sensors with compact design are generally costly [24]. Recently, a small body of work has explored model-based control methods for assisting STS movements [15], [25]. Liu *et al.* [25] used a simplified two-degree-of-freedom (2DoF) model to estimate the limped knee joint torque of the wearer and a knee-joint exoskeleton. Vantilt *et al.* [15] proposed a modelling method of a full lower limb exoskeleton to estimate its ankle, knee and hip joint torques during STS movements. In both works, a Kalman filter is used to estimate the joint angular velocities and accelerations for an inverse dynamic model.

Most of the existing control strategies for assisting elderly and patients with partial motor ability, focus on reducing the required muscular strengths of the wearer during normal-pattern STS movements [14], [15], [18], [19], [25]. For example, in [18], it has been shown that the muscle activities of the quadriceps of twelve healthy subjects can be reduced with the assistance of a knee-joint exoskeleton. In addition, some works further enhanced the wearer's joint stiffness with exoskeleton's assistance [14], [25]. In [15], authors developed a model-based control method of a full-lower limb exoskeleton to fully compensate for the exoskeleton dynamics including both gravity and inertia. Although lack of coordination/balance control represents a significant limiting factor impacting the STS movements with respect to wearers with partial motor ability [3], [7], [26], [27], this factor was rarely taken into account in the developed assistive strategies targeting this population [28]. Studies have revealed that abnormal STS strategies are commonly used by elderly and patients suffering from muscle weaknesses or musculoskeletal disorders [3], [7], [29]. For example, post-stroke patients may not be able to sufficiently shift their CoMs forward before seat-off, while they complete the knee joint extension when the hips are still extending [7]. Hence, only augmenting the wearer's joint torque/stiffness using a voluntary-motion assistive method might be insufficient for such population to ensure a successful STS due to their abnormal STS strategies caused by poor coordination between joints/muscles.

In this article, a novel impedance modulation control strategy of a lower limb exoskeleton is proposed for assisting wearers with partial motor ability during STS movements. The proposed strategy is aimed to reduce the required wearer's effort for performing a successful STS movement while avoiding two typical failed STS movements resulting from lack of balance/coordination, i.e., sitback and step. This is achieved by modulating the mechanical impedance of the human-exoskeleton system toward a desired one with lower impedance for wearer's effort reduction and higher virtual external impedance for balance reinforcement. Through partial compensation of the human-exoskeleton system impedance, including inertia and gravity, the required wearer's joint torques for performing a successful STS movement can be reduced while preserving the wearer's control priority. Meanwhile, a virtual quasi-stiffness force is added to the wearer's upper body to ensure the wearer's CoM placement within a correct support base. This can enhance the wearer's balance ability to cope with abnormal STS movements and to avoid STS failures.

The contributions of the paper can be summarized as follows. Firstly, a desired impedance model is designed to ensure both power assistance and balance reinforcement. The desired impedance model is adapted with wearer's posture and the STS speed such that an appropriate power and balance assistance by taking into account the wearer's lower-limb muscular ability and his/her STS strategies. Secondly, an impedance modulation structure is proposed to adapt the mechanical impedance of the human-exoskeleton system into the desired one. Apart from the desired impedance model, the impedance modulation structure includes two other parts: a human joint torque observer (HJTO) and a sliding mode-based controller (SMC). A nonlinear disturbance observer [30] is used as the HJTO to estimate the wearer's joint torques, which can accurately estimate the wearer's joint torques without using extra sensors, such as EMG sensors [31]. Thirdly, the robustness of the impedance modulation control strategy with respect to modelling uncertainties is theoretically analyzed. Lastly, the effectiveness of the proposed method is evaluated via simulations and experiments with four healthy subjects during four types of STS movements such as medium-speed, low-speed, sitback-like and step-like. The EMG signals of the

TABLE I: Modeling Symbols

Notation	*Description*
m_{h1}, m_{h2}, m_{h3}	Masses of the wearer's shank, thigh and HAT
m_{e1}, m_{e2}, m_{e3}	Masses of the exoskeleton shank, thigh and HAT
l_1, l_2, l_3	Lengths of the wearer's shank, thigh and HAT
k_{h1}, k_{h2}, k_{h3}	The coefficients of distribution of gravity for the wearer's shank, thigh and HAT respectively
k_{e1}, k_{e2}, k_{e3}	The coefficients of distribution of gravity for the exoskeleton shank, thigh and HAT respectively
I_{h1}, I_{h2}, I_{h3}	Inertias of the wearer's shank, thigh and HAT
I_{e1}, I_{e2}, I_{e3}	Inertias of exoskeleton shank, thigh and HAT
$\tau_{h,a}, \tau_{h,k}, \tau_{h,h}$	Torques developed by the wearer at the ankle, knee and hip joints, respectively
$\tau_{e,k}, \tau_{e,h}$	Torques generated by the exoskeleton at the knee and hip joints, respectively

related muscles are measured and show significant reduction when using the proposed method. To the best of our knowledge, this is the first method that can achieve both power assistance and balance reinforcement using a unified control structure to support the voluntary capabilities of individuals with partial motor ability during STS movements.

This article is an extended version of our previous conference publication [32] that further includes 1) balance reinforcement control; 2) an improved impedance reduction ratio function, which ensures appropriate power and balance assistance based on the wearer's STS posture and speed; 3) detailed analysis of the HJTO performance with respect to a conventional inverse dynamic model based method; 4) introducing an accurate parametric identification method; 5) theoretical analysis of the robustness with respect to modelling uncertainties; 6) detailed and extensive validation of the proposed approach via both simulations and experiments with four healthy subjects.

The rest of this article is organized as follows. Section II describes the human exoskeleton system during STS movements. In Section III, a desired impedance model is proposed. Section IV presents the detailed design of the impedance modulation control strategy as well as a parametric identification method. The associated theoretical analyses of stability and robustness are given as well. In Section V, the proposed method is evaluated via simulations and experiments, and Section VI concludes the article.

II. System Modeling

A schematic view of a subject wearing a lower-limb exoskeleton and performing STS transfer task is shown in Fig. 1. During the STS movement, the human body in the sagittal plane can be modeled using a triple inverted pendulum [33], [34]. The whole body includes three segments: shank-foot, thigh and HAT (Head-Arm-Torso). Correspondingly, a lower limb exoskeleton consisting of shank, thigh and torso segments, can also be modeled as a triple inverted pendulum. For the sake of simplicity, the exoskeleton's and subject's ankle, knee and hip joints movements are assumed synchronous (i.e., the connection between the exoskeleton and the subject is rigid) during STS movements. Meanwhile, only the STS movements during which the subject stands up from a chair without hand assistance are taken into account in this study.

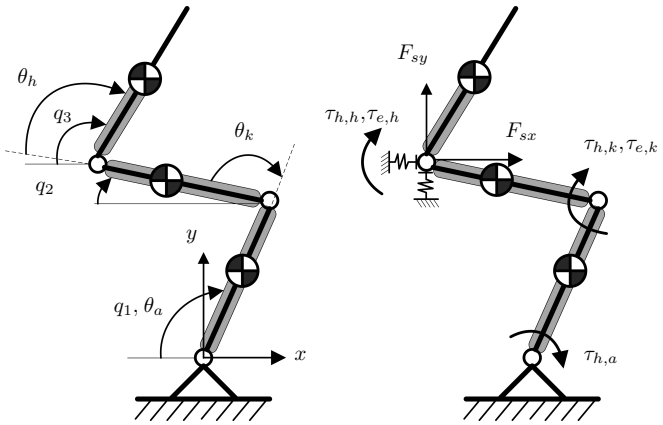


Fig. 1: Schematic view of a subject wearing an exoskeleton and achieving the STS movement in the sagittal plane. The exoskeleton is represented by the gray rounded rectangles.

Given that, a 3-DoF model of the human-exoskeleton is used as shown in Fig. 1. The exoskeleton, attached to the human body, is represented by the grey rounded rectangles. The physical parameters of each segment are listed in Table I. Using the Euler-Lagrange formalism [35], the dynamic model of the human-exoskeleton system is described by:

$$\boldsymbol{M}(\boldsymbol{q})\ddot{\boldsymbol{q}} + \boldsymbol{C}(\boldsymbol{q}, \dot{\boldsymbol{q}})\dot{\boldsymbol{q}} + \boldsymbol{G}(\boldsymbol{q}) = \boldsymbol{U} + \boldsymbol{J}_F^T \boldsymbol{F}, \tag{1}$$

where $\boldsymbol{q} = [q_1 \ q_2 \ q_3]^T$ represents the state vector of the ankle, knee and hip joint angles. $\boldsymbol{M}(\boldsymbol{q})$, $\boldsymbol{C}(\boldsymbol{q}, \dot{\boldsymbol{q}})$ and $\boldsymbol{G}(\boldsymbol{q})$ denote the inertia matrix, the Coriolis and centrifugal matrix, the gravitational vector, respectively. The seat force is modeled as an external force, $\boldsymbol{F}$, that acts on the hip joint of the human-exoskeleton. $\boldsymbol{J}_F$ is the Jacobian matrix. The input torque vector $\boldsymbol{U}$ is given as follows:

$$\boldsymbol{U} = \boldsymbol{U}_h + \boldsymbol{U}_e = \boldsymbol{R}\left(\begin{bmatrix} \tau_{h,a} \\ \tau_{h,k} \\ \tau_{h,h} \end{bmatrix} + \begin{bmatrix} 0 \\ \tau_{e,k} \\ \tau_{e,h} \end{bmatrix} \right). \tag{2}$$

$\boldsymbol{U}_h$ denotes the vector of torques generated by the wearer at the ankle, knee and hip joints. $\boldsymbol{U}_e$ represents the vector of torques exerted by the exoskeleton at the knee and hip joints level. Note that both ankle joints of the exoskeleton are passive. The transformation matrix $\boldsymbol{R}$ is given as follows:

$$\boldsymbol{R} = (\boldsymbol{J}_\Theta^{-1})^T, \tag{3}$$

where $\boldsymbol{J}_\Theta$ represents the transformation matrix from the joint space (θ_a, θ_k, θ_h) to the defined joint angle space (q_1, q_2, q_3) (see Fig. 1). Definitions of the matrices $\boldsymbol{J}_\Theta$, and $\boldsymbol{J}_F$ are given in Appendix A.

The main role of the seat force $\boldsymbol{F}$ is compensating for wearer's gravity in the sitting position. In this study, the seat force is supposed to fully compensate for the torques acting at the knee and ankle joints level by the body gravity in the sitting position (i.e., the wearer's knee and ankle joints are free ($\tau_{h,a} = \tau_{h,k} = 0$) in the sitting position). Meanwhile, this force should fade to zero when the position of the hip joint is higher than a certain height (i.e., seat-off point). In practice, however, the seat-off point is difficult to be detected using only joint angle information as the chair heights may change. On

the other hand, it is shown that the maximum vertical ground reaction force (GRF) time matches well the "seat-off" time [3]. Hence, the model of the seat force is designed as follows:

$$\boldsymbol{F} = [F_{sx}\ F_{sy}] = \beta_F \boldsymbol{F}_s, \tag{4}$$

with

$$\beta_F = 1 - F_{GRF}/F_{GRF,max}\ ,$$

where β_F is a positive ratio ($\beta_F \in [0\ 1]$). F_{GRF} denotes the measured vertical GRF, while $F_{GRF,max}$ represents the maximum vertical GRF. $\boldsymbol{F}_s$ is the force that can fully compensate for the torques at the wearer's ankle and knee joints level induced by the body gravity, and is calculated as follows:

$$\boldsymbol{F}_s = (\boldsymbol{H}\boldsymbol{R}^{-1}\boldsymbol{J}_F^T)^{-1}\boldsymbol{H}\boldsymbol{R}^{-1}\boldsymbol{G}(\boldsymbol{q}), \tag{5}$$

where $\boldsymbol{H}$ is a constant matrix used to extract the ankle and knee joint torques from the torque vector $\boldsymbol{U}$. The definition of the matrix $\boldsymbol{H}$ is given in Appendix A.

III. Desired Impedance Modulation

In this study, we aim to address two main problems affecting the STS movement of the elderly and patients suffering from neurological disorders: lower limb muscle weakness and insufficient balance control ability. To this end, an impedance modulation method is proposed through two steps: impedance compensation and balance control reinforcement.

1) Impedance Compensation: To ensure a successful STS movement, significant lower limb joint torques are required [36], [37] (normalized peak flexion/extension torque over bodyweight and body height: hip joint 0.45 Nm/kg/m and knee joint 0.58 Nm/kg/m [37]), which makes the STS movement a challenging task for individuals with lower limb muscular weakness. With the support of an exoskeleton, an efficient method for reducing the required human joint torques during STS movements is to partially compensate for the gravity and inertia (i.e., impedance) of the human-exoskeleton system. In other words, a desired impedance lower than the original one of the wearer's body is expected to reduce the required wearer's effort. A major advantage of this method is that the STS movement is still dominated by the wearer while the exoskeleton provides appropriate assistance according to the wearer's muscular torques. Moreover, the desired impedance model can be designed based on the wearer's lower limb motor ability, which is usually assessed using the well-known five-times-sit-to-stand (FTSTS) test [38]. Researches in the literature show that an elderly with relatively longer standing-up time is usually associated with an increasing factor of disability, morbidity and fall risk [38]. According to the human-exoskeleton model (1), a wearer's lower-limb motor ability based impedance compensation model is proposed as follows:

$$\boldsymbol{\lambda}_1(\boldsymbol{M}(\boldsymbol{q})\ddot{\boldsymbol{q}}_r + \boldsymbol{C}(\boldsymbol{q},\dot{\boldsymbol{q}})\dot{\boldsymbol{q}}_r) + \boldsymbol{\lambda}_2\boldsymbol{G}(\boldsymbol{q}) = \boldsymbol{R}\hat{\boldsymbol{\tau}}_h + \boldsymbol{\lambda}_2\boldsymbol{J}_F^T\boldsymbol{F}, \tag{6}$$

with

$$\boldsymbol{\lambda}_1 = \boldsymbol{\lambda}_2 = \mathrm{diag}(1, \lambda_k, \lambda_h), \quad \lambda_k, \lambda_h \in (0,\ 1], \tag{7}$$

where the vectors $\ddot{\boldsymbol{q}}_r$ and $\dot{\boldsymbol{q}}_r$ denote the generated reference joint accelerations and velocities, respectively. $\hat{\boldsymbol{\tau}}_h$ represents the estimated wearer's joint torques vector. λ_h and λ_k represent the assistive ratios at the hip and knee joints level, respectively. In this study, same assistive ratios are used at the hip and knee joints, i.e., $\lambda_h = \lambda_k$, and are expressed as follows:

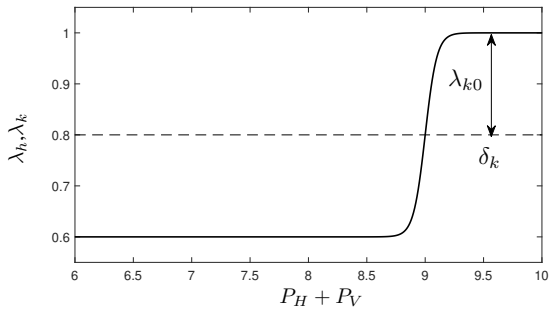


Fig. 2: One example of the function of λ_h and λ_k (8).

$$\lambda_h = \lambda_k = \lambda_{k0}\tanh(s_k(p_H + p_V) + 1) + \delta_k, \tag{8}$$

with

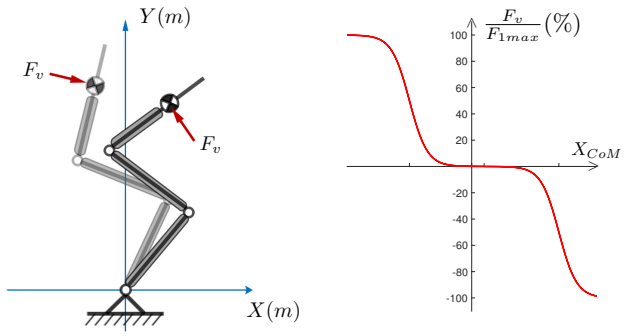
$$p_H = g(h_{hHAT} - h_{th}) \tag{9}$$

$$p_V = \kappa_v \tanh(s_v(v_{max} - v_{th})) + \kappa_v \tag{10}$$

where δ_k and λ_{k0} are two constants determining the middle and range of ratios λ_h and λ_k, respectively. h_{hHAT} denotes the vertical linear position and of the CoM of the wearer's HAT. v_{max} represents the maximum vertical linear velocity of the CoM of the wearer's HAT over the period from the start of the STS to the current sample. g is the gravitational acceleration. h_{th} is the upper bound of h_{hHAT} (in standing posture). κ_v is a constant and v_{th} is a threshold, which can be selected based on healthy people's STS speeds. s_k and s_v are two sensitivity coefficients. An example of the function (8) is illustrated in Fig. 2. When the wearer stands up with a relatively low speed which is the case he/she lacks motor ability, the desired impedance keeps low until the wearer's posture is approaching the standing posture, i.e., h_{hHAT} is close to h_{th}. Meanwhile, large standing up speeds also induce a quick increase in the parameters λ_h and λ_k. In this study, it is assumed that limited/no assistance is needed for individuals who are able to stand up from a chair with a normal or even fast speed [38].

2) Balance Reinforcement Control: Since the human-exoskeleton model is close to a 3-DoF inverse pendulum model (see Fig. 1) during the STS movement, balance control is also of great importance to ensure a successful STS movement. Apart from reducing the wearer's effort, an efficient coordination among the lower limb joint motions is highly required. Given that, a virtual stiffness force is introduced at the wearer's HAT level to reinforce his/her balance control ability (see Fig. 3). The proposed virtual stiffness force, F_v, is assumed to be always normal to the wearer's HAT and acts at its CoM:

$$F_v = \begin{cases} -F_{1max}\tanh(K_{s1}(X_{CoM} - x_{c1})), & \text{if } X_{CoM} < x_{c1} \\ 0, & \text{if } x_{c1} \le X_{CoM} \le x_{c2} \\ -F_{2max}\tanh(K_{s2}(X_{CoM} - x_{c2})), & \text{if } X_{CoM} > x_{c2} \end{cases} \tag{11}$$



(a) (b)

Fig. 3: Principle diagram of the virtual stiffness force (VSF). (a) VSF directions, (b) an example curve of the VSF (with $F_{1max} = F_{2max}$ and $K_{s1} = K_{s2}$).

where F_{1max} and F_{2max} represent the maximum virtual stiffness forces, and K_{s1} and K_{s2} are the sensitive gains. X_{CoM} denotes the horizontal position of the CoM of the human-exoskeleton system in the sagittal plane. x_{c1} and x_{c2} respectively represent the virtual left and right margins of the X_{CoM}, with $x_{c1} \leq 0 \leq x_{c2}$.

The virtual stiffness force (11) is used to guarantee that the horizontal projection of the CoM of the human-exoskeleton system, X_{CoM}, locates in a given range (i.e., $[x_{c1} \;\; x_{c2}]$) with respect to the foot position (i.e., the origin) as shown in Fig. 3. If $x_{c1} \leq X_{CoM} \leq x_{c2}$, the virtual stiffness force is zero and the wearer can freely adjust his/her posture, otherwise, a significant stiffness force is introduced at the wearer's HAT level to prevent loss of balance (see Fig. 3).

By combining the virtual stiffness force and the impedance compensation (i.e., (6)), the desired impedance model can be expressed as follows:

$$\boldsymbol{\lambda}_1(\boldsymbol{M}(\boldsymbol{q})\ddot{\boldsymbol{q}}_r + \boldsymbol{C}(\boldsymbol{q},\dot{\boldsymbol{q}})\dot{\boldsymbol{q}}_r) + \boldsymbol{\lambda}_2\boldsymbol{G}(\boldsymbol{q}) = \boldsymbol{R}(\hat{\boldsymbol{\tau}}_h + \boldsymbol{\tau}_v) + \boldsymbol{\lambda}_2\boldsymbol{J}_F^T\boldsymbol{F} \tag{12}$$

with

$$\boldsymbol{\tau}_v = \frac{F_{GRF}(1-\lambda_h)}{F_{GRF,max}(1-\delta_k-\lambda_{k0})}[0 \;\; 0 \;\; F_v l_3 k_{h3}]^T \tag{13}$$

where $\boldsymbol{\tau}_v$ represents the virtual torque caused by the virtual stiffness force (11), $\|\boldsymbol{\tau}_v\| < \varepsilon_v$. ε_v is a positive constant. The virtual torque $\boldsymbol{\tau}_v$ is also defined as a function of the ground reaction force F_{GRF} and the assistive ratio λ_h. Note that the virtual torque is considered to be zero when the wearer sits on a chair, i.e., $F_{GRF} = 0$, or when the assistive ratio $\lambda_h = 1$.

IV. Impedance Modulation Control for Multi-joint Movements

To ensure that the human-exoskeleton system (1) behaves according to the desired impedance model (12), an impedance modulation control structure is proposed as shown in Fig.4. The impedance modulation model consists of three parts: a nonlinear HJTO, a SMC-based controller as well as a desired admittance model (i.e., the inverse desired impedance model). The principle of this structure is as follows: the HJTO is used to estimate the wearer's joint torques ($\boldsymbol{U}_h$) and the SMC-based controller is used to track the reference motion trajectory ($\boldsymbol{q}_r$) generated by the desired impedance model. The original human exoskeleton model can be adapted to the desired impedance model with respect to the estimated wearer's torques ($\hat{\boldsymbol{U}}_h$) if the following conditions are satisfied: 1) the HJTO can accurately estimate the wearer's joint torque (i.e., $\hat{\boldsymbol{U}}_h = \boldsymbol{U}_h$); 2) the SMC-based controller shows a high tracking accuracy (i.e., $\boldsymbol{q} = \boldsymbol{q}_r$). In the following subsections, we present the design of the impedance modulation control structure (see Fig.4) as well as its characteristics, performance and robustness with respect to modeling uncertainties.

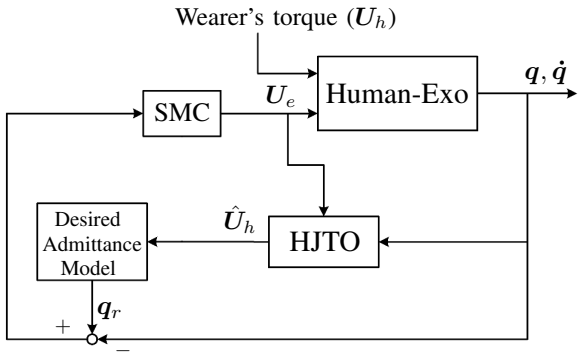


Fig. 4: Impedance modulation structure. ($\hat{\boldsymbol{U}}_h$: estimated wearer's torques; $\boldsymbol{U}_e$: assistive torques; $\boldsymbol{q}_r$: desired joint angles).

A. Human Joint Torque Observer (HJTO)

The HJTO is developed using the disturbance observer technique [39], [30], i.e., the wearer's joint torques $\boldsymbol{U}_h$ are considered as external disturbances for the human-exoskeleton system. Correspondingly, the dynamic model (1), can be transformed into a nominal model with an additional disturbance term, $\boldsymbol{U}_h$:

$$\boldsymbol{M}(\boldsymbol{q})\ddot{\boldsymbol{q}} + \boldsymbol{C}(\boldsymbol{q},\dot{\boldsymbol{q}})\dot{\boldsymbol{q}} + \boldsymbol{G}(\boldsymbol{q}) = (\boldsymbol{U}_e + \boldsymbol{J}_F^T\boldsymbol{F}) + \boldsymbol{U}_h. \tag{14}$$

The HJTO is designed as follows:

$$\begin{cases} \dot{\boldsymbol{z}} &= -L(\boldsymbol{q},\dot{\boldsymbol{q}})\boldsymbol{z} + L(\boldsymbol{q},\dot{\boldsymbol{q}})(\boldsymbol{C}(\boldsymbol{q},\dot{\boldsymbol{q}})\dot{\boldsymbol{q}} + \boldsymbol{G}(\boldsymbol{q}) \\ & \quad -\boldsymbol{U}_e - \boldsymbol{J}_F^T\boldsymbol{F} - \boldsymbol{p}(\boldsymbol{q},\dot{\boldsymbol{q}})), \\ \hat{\boldsymbol{U}}_h &= \boldsymbol{z} + \boldsymbol{p}(\boldsymbol{p},\dot{\boldsymbol{q}}), \end{cases} \tag{15}$$

where $\hat{\boldsymbol{U}}_h$ denotes the estimated joint torques vector generated by the human. $\boldsymbol{z}$ is an auxiliary variable used to avoid the acceleration measurement. The observer gain matrix $L(\boldsymbol{q},\dot{\boldsymbol{q}})$ and the vector $\boldsymbol{p}(\boldsymbol{q},\dot{\boldsymbol{q}})$ satisfy:

$$\begin{cases} L(\boldsymbol{q},\dot{\boldsymbol{q}}) = \boldsymbol{X}^{-1}\boldsymbol{M}^{-1}(\boldsymbol{q}) \\ \boldsymbol{p}(\boldsymbol{q},\dot{\boldsymbol{q}}) = \boldsymbol{X}^{-1}\dot{\boldsymbol{q}} \end{cases} \tag{16}$$

Let us define the disturbance tracking error as $\tilde{\boldsymbol{U}}_h = \boldsymbol{U}_h - \hat{\boldsymbol{U}}_h$. From (14) - (16), the error dynamics of the tracking disturbance can be obtained as follows:

$$\dot{\tilde{\boldsymbol{U}}}_h = \dot{\boldsymbol{U}}_h - L(\boldsymbol{q},\dot{\boldsymbol{q}})\tilde{\boldsymbol{U}}_h. \tag{17}$$

The following proposition addresses the tracking performance of HJTO (15) for system (14).

Proposition 1. Consider the human-exoskeleton system subjects to the disturbances $\boldsymbol{U}_h$ (i.e., the wearer's joint torques). The HJTO is given in (15) with the observer gain matrix $L(\boldsymbol{q}, \dot{\boldsymbol{q}})$ and auxiliary vector $\boldsymbol{p}(\boldsymbol{q}, \dot{\boldsymbol{q}})$ defined in (16). The matrix $\boldsymbol{X}$ is invertible and there exists a positive definite and symmetric matrix $\boldsymbol{\Gamma}$, such that [30] :

$$\boldsymbol{X} + \boldsymbol{X}^T - \boldsymbol{X}^T \dot{\boldsymbol{M}}(\boldsymbol{q}) \boldsymbol{X} \geq \boldsymbol{\Gamma} \ , \tag{18}$$

1) If the rates of change of the wearer's joint torques are negligible (i.e., $\dot{\boldsymbol{U}}_h \approx 0$), the tracking errors of the wearer's joint torques, $\tilde{\boldsymbol{U}}_h$, converge exponentially to zero for any $\tilde{\boldsymbol{U}}_h \in R^n$.
2) If the rates of change of the wearer's joint torques are bounded (i.e., $\|\dot{\boldsymbol{U}}_h\| < \varepsilon$), the tracking errors of the wearer's joint torques, $\tilde{\boldsymbol{U}}_h$, are globally uniformly ultimately bounded.

Proof: Detailed proof is refereed to [30]. □

In practice, the matrix $\boldsymbol{X}$ can be chosen as a diagonal matrix for simplicity. A possible analytical solution of $\boldsymbol{X}$ suggested in [30] is given by

$$\boldsymbol{X}^{-1} = \frac{1}{2}(\zeta + 2\beta_o \sigma_1)\boldsymbol{I}, \tag{19}$$

where $\boldsymbol{I}$ represents the identity matrix. β_o is the minimum convergence rate of the human joint tracking error. ζ and σ_1 are two constants that satisfy the following conditions:

$$\| \boldsymbol{M}(\boldsymbol{q}) \| \leq \sigma_1, \ \| \dot{\boldsymbol{M}}(\boldsymbol{q}), \| \leq \zeta \tag{20}$$

During the STS movement, the velocities of the wearer's joint torques are bounded (i.e. $\|\dot{\boldsymbol{U}}_h\| < \varepsilon$). As pointed out in [30], the tracking errors converge with an exponential rate, $\frac{(1-\eta)\Gamma}{2\sigma_1 \|\boldsymbol{X}\|^2}$, to a ball with a radius of $\frac{2\varepsilon\sigma_1\|\boldsymbol{X}\|^2}{\eta\Gamma}, 0 < \eta < 1$. Γ represents a positive value. One can notice that there is a trade-off between the accuracy of the estimated wearer's joint torques and the noise amplification when using the HJTO. In this study, the convergence rate β_o is designed based on the main frequency range (0.5-0.05 Hz) of STS movements.

Remark 1. To estimate wearer's joint torques, a common model-based method is to first use a Kalman filter to estimate joint velocities/accelerations, and then, use them as inputs of an inverse dynamic model, e.g., [15], [40]. Generally, a constant acceleration model is used within the Kalman filter, and the joint velocities and accelerations are assumed to be subject to noises with given covariances. The advantage of this method lies in its ability to reduce the influence of the measurement noises while ensuring a relatively low phase lag. However, the aforementioned Kalman filter fails to guarantee the phase consistency of the estimated joint angle, velocity and acceleration. Unlike the torque control based method used in [15], a SMC-based position controller (see Section IV-B) is used in this study to ensure an accurate achievement of the desired impedance (12). Phase differences among the estimated joint angle, velocity and acceleration may cause unexpected assistive torques (see Section V-C1). Given that, the nonlinear disturbance observer (15) is used. Traditional nonlinear disturbance observers usually assume that the change rate of the disturbance is zero or slow [39]. However, the change rates of the wearer's joint torques, which are considered as disturbances to the human-exoskeleton system (16), can be relatively large during STS movements and its dynamics could not be neglected. The designed HJTO, (15) and (19), can effectively estimate the fast-varying wearer's joint torques [30].

B. Design of the Sliding Mode based Controller (SMC)

In order to ensure an accurate tracking of the reference motion intention, $\boldsymbol{q}_r$, computed using the desired impedance model (12), an SMC-based controller with feed-forward compensation is used.

Let us define:

$$\boldsymbol{s} = c_1 \boldsymbol{e} + \dot{\boldsymbol{e}}, \quad \boldsymbol{e} = \boldsymbol{q} - \boldsymbol{q}_r \tag{21}$$

where $\boldsymbol{s}$ represents a virtual error vector. c_1 is a positive constant.

The multi-joint SMC-based controller is designed as follows:

$$\begin{aligned} \boldsymbol{U}_e = & -c_1(\boldsymbol{M}(\boldsymbol{q})\dot{\boldsymbol{e}} + \boldsymbol{C}(\boldsymbol{q}, \dot{\boldsymbol{q}})\boldsymbol{e}) + (1-\lambda_1)(\boldsymbol{M}(\boldsymbol{q})\ddot{\boldsymbol{q}}_r \\ & + \boldsymbol{C}(\boldsymbol{q}, \dot{\boldsymbol{q}})\dot{\boldsymbol{q}}_r) + (1-\lambda_2)(\boldsymbol{G}(\boldsymbol{q}) - \boldsymbol{J}_F^T \boldsymbol{F}) \\ & - \sigma_s \text{sat}(\boldsymbol{s}) - \lambda_s \boldsymbol{s}, \end{aligned} \tag{22}$$

where σ_s is a positive constant. sat$(\cdot)$ denotes a saturation function (sat$(\cdot) \in [-1, 1]$). Note that ankle joints are only controlled by the wearer (see (2)) thus, the desired ankle joint angle corresponds to the current ankle joint angles (i.e., $\boldsymbol{q}_{r,[1]} = \boldsymbol{q}_{[1]}$, $\boldsymbol{e}_{[1]} = 0$ and $\boldsymbol{U}_{h,[1]} = 0$).

The stability of the proposed controller (22) is addressed using the following proposition.

Proposition 2. The exoskeleton controller is given by (22), and $\boldsymbol{e}_{[1]} = 0$, $\sigma_s > \frac{2\varepsilon\sigma_1\|\boldsymbol{X}\|^2}{\eta\Gamma} + \varepsilon_v$. The virtual tracking error, $\boldsymbol{s}$, converges exponentially to zero for all $\boldsymbol{s}(0) \in R^3$. Note that $\boldsymbol{\tau}_v$ is zero when the horizontal position of the CoM of the human-exoskeleton system, X_{CoM}, is in the range $[x_{c1}\ x_{c2}]$.

Proof: The proof is given in Appendix B. □

C. Robustness with Respect to Modeling Uncertainties

Considering the modeling uncertainties, the real human-exoskeleton system model can be represented as follows:

$$\boldsymbol{M}^*(\boldsymbol{q})\ddot{\boldsymbol{q}} + \boldsymbol{C}^*(\boldsymbol{q}, \dot{\boldsymbol{q}})\dot{\boldsymbol{q}} + \boldsymbol{G}^*(\boldsymbol{q}) = \boldsymbol{U} = \boldsymbol{U}_e + \boldsymbol{U}_h + \boldsymbol{J}_F^T \boldsymbol{F}, \tag{23}$$

where the parameter matrices satisfy:

$$\boldsymbol{M}^*(\boldsymbol{q}) = \boldsymbol{M}(\boldsymbol{q}) + \Delta\boldsymbol{M}(\boldsymbol{q}), \tag{24}$$

$$\boldsymbol{C}^*(\boldsymbol{q}, \dot{\boldsymbol{q}}) = \boldsymbol{C}(\boldsymbol{q}, \dot{\boldsymbol{q}}) + \Delta\boldsymbol{C}(\boldsymbol{q}, \dot{\boldsymbol{q}}), \tag{25}$$

$$\boldsymbol{G}^*(\boldsymbol{q}) = G(\boldsymbol{q}) + \Delta G(\boldsymbol{q}). \tag{26}$$

For both the identified and real human-exoskeleton systems, it is reasonable to assume that the parameter matrices have the following properties:

Property 1. The inertia matrices are symmetric and positive definite, i.e. we have:

$$\begin{aligned} & \xi^T \boldsymbol{M}^*(\boldsymbol{q})\xi = \xi^T (\boldsymbol{M}^*(\boldsymbol{q}))^T \xi > 0 \\ & \xi^T \boldsymbol{M}(\boldsymbol{q})\xi = \xi^T (\boldsymbol{M}(\boldsymbol{q}))^T \xi > 0, \quad \forall \boldsymbol{q}, \xi \in R^n. \end{aligned} \tag{27}$$

Property 2. The matrices $\frac{1}{2}\dot{\boldsymbol{M}}^*(\boldsymbol{q}) - \boldsymbol{C}^*(\boldsymbol{q},\dot{\boldsymbol{q}})$ and $\frac{1}{2}\dot{\boldsymbol{M}}(\boldsymbol{q}) - \boldsymbol{C}(\boldsymbol{q},\dot{\boldsymbol{q}})$ are all skew-symmetric and can be shown that:

$$\begin{aligned}&\xi^T(\frac{1}{2}\dot{\boldsymbol{M}}^*(\boldsymbol{q}) - \boldsymbol{C}^*(\boldsymbol{q},\dot{\boldsymbol{q}}))\xi = 0\\ &\xi^T(\frac{1}{2}\dot{\boldsymbol{M}}(\boldsymbol{q}) - \boldsymbol{C}(\boldsymbol{q},\dot{\boldsymbol{q}}))\xi = 0, \quad \forall \boldsymbol{q},\dot{\boldsymbol{q}},\xi \in R^n.\end{aligned} \tag{28}$$

Property 3. Assume that the gravitational potential functions of the real and identified human-exoskeleton systems are $P_E^*(\boldsymbol{q}) > 0$ and $P_E(\boldsymbol{q}) > 0$. Thus, the gravitational terms in the corresponding models satisfy:

$$G^*(\boldsymbol{q}) = \frac{\partial P_E^*(\boldsymbol{q})}{\partial \boldsymbol{q}}, \quad G(\boldsymbol{q}) = \frac{\partial P_E(\boldsymbol{q})}{\partial \boldsymbol{q}}. \tag{29}$$

Property 4. The elastic potential function of the virtual stiffness torque is assumed as $P_V(\boldsymbol{q})$. Therefore, we have:

$$\boldsymbol{R}\boldsymbol{\tau}_v(\boldsymbol{q}) = \frac{\partial P_V(\boldsymbol{q})}{\partial \boldsymbol{q}}. \tag{30}$$

Lemma 1. The modeling uncertainty terms $\Delta\boldsymbol{M}(\boldsymbol{q})$, $\Delta\boldsymbol{C}(\boldsymbol{q},\dot{\boldsymbol{q}})$ and $\Delta G(\boldsymbol{q})$ also have the similar properties, i.e. we have:

$$\xi^T\Delta\boldsymbol{M}(\boldsymbol{q})\xi = \xi^T(\Delta\boldsymbol{M}(\boldsymbol{q}))^T\xi > 0, \quad \forall \boldsymbol{q},\xi \in R^n \tag{31}$$

$$\xi^T(\frac{1}{2}\Delta\dot{\boldsymbol{M}}(\boldsymbol{q}) - \Delta\boldsymbol{C}(\boldsymbol{q},\dot{\boldsymbol{q}}))\xi = 0, \quad \forall \boldsymbol{q},\dot{\boldsymbol{q}}\xi \in R^n \tag{32}$$

$$\Delta G(\boldsymbol{q}) = \frac{\partial(P_E^*(\boldsymbol{q}) - P_E(\boldsymbol{q}))}{\partial \boldsymbol{q}}. \tag{33}$$

Proof: Lemma 1 can be easily obtained from (24) to (26). □

Note that the real system model (23) can be rewritten as follows:

$$\begin{aligned}\boldsymbol{M}(\boldsymbol{q})\ddot{\boldsymbol{q}} + \boldsymbol{C}(\boldsymbol{q},\dot{\boldsymbol{q}})\dot{\boldsymbol{q}} + \boldsymbol{G}(\boldsymbol{q}) = \boldsymbol{U} =& \boldsymbol{U}_e + \boldsymbol{U}_h + \boldsymbol{J}_F^T\boldsymbol{F}\\ &+ \boldsymbol{T}_d(\boldsymbol{q},\dot{\boldsymbol{q}},\ddot{\boldsymbol{q}}),\end{aligned} \tag{34}$$

where the lumped disturbance is given by:

$$\boldsymbol{T}_d(\boldsymbol{q},\dot{\boldsymbol{q}},\ddot{\boldsymbol{q}}) = -\Delta\boldsymbol{M}(\boldsymbol{q})\ddot{\boldsymbol{q}} - \Delta\boldsymbol{C}(\boldsymbol{q},\dot{\boldsymbol{q}})\dot{\boldsymbol{q}} - \Delta\boldsymbol{G}(\boldsymbol{q}). \tag{35}$$

Actually, the lumped disturbance $\boldsymbol{T}_d(\boldsymbol{q},\dot{\boldsymbol{q}},\ddot{\boldsymbol{q}})$ cannot be excluded in the estimated wearer's torques $\hat{\boldsymbol{U}}_h$, because we use the nominal system parameters in the nonlinear disturbance observer (15). Thus, we have the following approximation in the steady state of trajectory tracking control:

$$\hat{\boldsymbol{U}}_h = \boldsymbol{U}_h + \boldsymbol{T}_d(\boldsymbol{q},\dot{\boldsymbol{q}},\ddot{\boldsymbol{q}}), \tag{36}$$

where $\boldsymbol{U}_h$ is the generalized torques vector obtained from the actual wearer's muscle strength. Therefore, the real desired impedance model can be written as follows:

$$\begin{aligned}\boldsymbol{\lambda}_1(\boldsymbol{M}(\boldsymbol{q})\ddot{\boldsymbol{q}}_r + \boldsymbol{C}(\boldsymbol{q},\dot{\boldsymbol{q}})\dot{\boldsymbol{q}}_r) + \boldsymbol{\lambda}_2\boldsymbol{G}(\boldsymbol{q}) = \boldsymbol{U}_h + \boldsymbol{R}\boldsymbol{\tau}_v(\boldsymbol{q})\\ + \boldsymbol{T}_d(\boldsymbol{q},\dot{\boldsymbol{q}},\ddot{\boldsymbol{q}}).\end{aligned} \tag{37}$$

The scaling matrices $\boldsymbol{\lambda}_1$ and $\boldsymbol{\lambda}_2$ are related to the desired robotic assistance and satisfy:

$$\|\boldsymbol{\lambda}_1\|_\infty < 1, \quad \|\boldsymbol{\lambda}_2\|_\infty < 1. \tag{38}$$

From (37), we can observe that even there is no human joint torques $\boldsymbol{U}_h$, the reference trajectory $\boldsymbol{q}_r$ might be unstable due to the lumped disturbance. To guarantee the safety of wearer, the stability of reference trajectory $\boldsymbol{q}_r$ should be robust to model uncertainties. The following theorem gives the sufficient condition of this robustness.

Proposition 3. For $\forall \boldsymbol{q}_r \in R^n$, if the following inequalities:

$$\begin{aligned}&\boldsymbol{\lambda}_1\boldsymbol{M}(\boldsymbol{q}_r) + \Delta\boldsymbol{M}(\boldsymbol{q}_r) > 0,\\ &(\boldsymbol{\lambda}_2 - \boldsymbol{I})P_E(\boldsymbol{q}_r) + P_E^*(\boldsymbol{q}_r) + P_V(\boldsymbol{q}_r) > 0\end{aligned} \tag{39}$$

hold, then the equilibrium $\boldsymbol{q}_r - \boldsymbol{q}_{r0}$ is stable with $\boldsymbol{\lambda}_2\boldsymbol{G}(\boldsymbol{q}_{r0}) + \Delta\boldsymbol{G}(\boldsymbol{q}_{r0}) + \boldsymbol{R}\boldsymbol{\tau}_v(\boldsymbol{q}_{r0}) = 0$.

Proof: The proof is given in Appendix C. □

D. Parametric Identification of Human-Exoskeleton System

The robustness analysis detailed in Section IV-C shows that an accurate wearer-exoskeleton system model can enable not only a desired assistance but also a large assistive ratio (see (39)). In our previous work [41], an identification method was proposed to identify a human-exoskeleton system composed of 20-DoF and 11 rigid segments. In this study, a simplified 3-DoF model (1) is considered to reproduce STS movements. The exoskeleton is not actuated at the ankle joint and cannot therefore support its own weight. Consequently, to identify its inertial parameters, two experiments are conducted. In the first experiment, the wearer's dynamics is identified when the human is not wearing the exoskeleton, while the second one is conducted to identify the dynamics of the entire human-exoskeleton system.

To identify the human-exoskeleton system, (1) is further rewritten linearly relatively to the inertial parameters using the so-called regressor matrice $\mathbf{W}$ [41]:

$$\mathbf{W}\boldsymbol{\Phi} = \begin{bmatrix}\mathbf{W}_H & \mathbf{0}\\ \mathbf{W}_H & \mathbf{W}_E\end{bmatrix}\boldsymbol{\Phi} = \mathbf{J}_w^T\mathbf{F}_{f,m} \tag{40}$$

where $\mathbf{W}_H$ corresponds to the collected data when the wearer is not wearing the exoskeleton and $\mathbf{W}_E$ corresponds to those when the subject is wearing the exoskeleton. $\boldsymbol{\Phi} = [\boldsymbol{\Phi}_1^T \cdots \boldsymbol{\Phi}_6^T]^T$ is the (18×1) vector of inertial parameters of both human and human-exoskeleton systems to identify. For each link i, three inertial parameters are expressed in the joint frame $\boldsymbol{\Phi}_i = \begin{bmatrix}M_i & MX_i & I_{zi}\end{bmatrix}$, where M_i is the mass, MX_i the first moment of inertia along the link, and I_{zi} the segment inertia with respect to the corresponding joint. $\mathbf{F}_{f,m} = \begin{bmatrix}F_Y & M_Z\end{bmatrix}^T$ denotes the external vertical force F_Y and moment M_z. $\mathbf{J}_w$ is the Jacobian matrix that maps the external force and moment to the root-link (i.e., the feet).

Since $\mathbf{W}$ is not a full column rank matrix, a least-squares based approach to solve (40) would give an infinity of solutions. Fortunately, (40) can be rewritten using the *so-called* base parameters (BP) as defined in [42] to obtain a full column rank regressor. Thus, the vector $\boldsymbol{\Phi}_b$ is the minimal set of identifiable inertial parameters required to describe the dynamics of the system. The computation of these parameters consists in finding a subset $\mathbf{W}_b$ of $\mathbf{W}$ that is a full column rank matrix [43]. For n samples of time, the identification problem can be formulated as follows:

$$\bar{\mathbf{W}}_b\boldsymbol{\Phi}_b = \bar{\mathbf{F}} \tag{41}$$

A vector $\mathbf{\Phi}_b^*$ of identified BP can be obtained using a weighted Moore-Penrose pseudo-inverse matrix to get the least-squares solution of equation (41) [44]. However, if the objective is to estimate the joint torques of both the wearer and the exoskeleton, the whole set of inertial parameters $\mathbf{\Phi}$ is necessary. In the present study, a constrained quadratic programming (QP) approach developed by our group [33], is used; this approach is formulated in Appendix D.

V. Simulations and Experiments

A. Experimental Setup

The experiments are implemented using the Angeleg exoskeleton, developed by SG Mechatronics, Korea (see Fig. 5). This exoskeleton consists of four parts: exoskeletal frames, series elastic actuators (SEAs), sensors, and a controller backpack with a battery inside. The total weight of the exoskeleton is 13 Kg. Each leg of the Angeleg exoskeleton has 7 DoFs including 3 DoFs at the hip and ankle joints level (i.e., adduction/abduction, flexion/extension, and rotation) and 1 DoF at the knee joint level (i.e., flexion/extension). The hip and knee joint flexion/extension movements are powered by four SEA actuators [45] while the remaining DoFs are passive. The output torque of each actuator can be measured using a spring-embedded gear in the SEA and the maximum output torque of each SEA is 18Nm. A PID with feedforward controller [46] is used as the low-level torque controller to ensure high-precision assistive torques for performing STS movements (magnitude response: -0.07−-0.88dB during 0.1−1Hz). The maximum joint speed of each SEA is 66.4 rpm. Each hip/knee joint is equipped with a 13-bit encoder (AVAGO Technologies, USA) measuring the associated joint angle. The ankle joint angle is measured using an IMU sensor (Xsens, Netherlands) attached to the left leg shank of the exoskeleton. The measured joint angles are lowpass filtered at 2Hz using a 2nd-order Butterworth filter.

An air-pressure based insole sensor is placed in each shoe to measure the GRF, F_{GRF} [47]. The maximum vertical GRF, $F_{GRF,max}$, in (4) is measured during a simple calibration process, in which the wearer is asked to stay in a static standing posture for 5 seconds while wearing the exoskeleton. Then, the $F_{GRF,max}$ is set as $0.875F_{GRF,standing}$, where $F_{GRF,standing}$ is the average measured GRF using the air-pressure based insoles. The ratio of 0.875 is used to take into account the measurement changes with the horizontal movement of the CoM, ensuring thus the chair's support is zero after the "seat-off" event. In comparison to the GRF measured using a 9N accurate Wii Balance Board (WIIBB, Nintendo), the accuracy of the calibrated GRF, $F_{GRF} \in [0\ F_{GRF,max}]$, measured using the air-pressure based insoles is 25.2N. This accuracy is sufficient to ensure an effective detection of the changing profile of the GRF (i.e., β_F) around the seat-off period.

A NI^{TM} Single-Board RIO is used to synchronize the sensor data and control the SEA actuators. The control law is deployed using LabVIEW and runs at 1 KHz.

B. Human-Exoskeleton Parameters

Four healthy male subjects (age: 27 ± 5 years old; height: 175.8 ± 5.7 cm; weight: 66.8 ± 5.4 Kg) participated in the experiments. Each subject was informed of the experimental protocols approved by Henri-Mondor Hospital, France, and gave his consent before participating in the experiments.



Fig. 5: Parametric identification: a subject is performing a squat-like motions while wearing the exoskeleton; a stereophotogrammetric system and a Wii balance board are used to collect kinematics and dynamometrics data, respectively.

Kinematics and dynamometrics data were measured using a stereophotogrammetric system (Optitrack, Flex 13) and a WIIBB, respectively. A set of six retro-reflective markers were placed on the subjects to fit the model presented in Fig. 5 and to estimate the corresponding joint angles. Joint velocities and accelerations were obtained using centred differences. The WIIBB allows measuring the external force F_Y and the moment M_Z along the vertical and lateral axes, respectively. Note that the WIIBB has been proven accurate enough to perform dynamics identification of a planar model of human [33]. All measured data were low-pass filtered at 5 Hz using a zero-phase 5th-order Butterworth filter.

The identification process was done in two steps. First, the subject was asked to perform some exciting motions without wearing the exoskeleton and then to perform the similar motions while wearing the exoskeleton. The retained exciting motions of two minutes duration approximately were shown to the subject. These motions were continuous and composed of 10 squats performed at different velocities, 10 oscillations of the hip/trunk and 10 oscillations of the ankle. These motions were considered as exciting since the condition number of the base parameter regressor matrix was relatively low ($cond(\mathbf{W}_b) = 36$).

The identified inertial parameters for each subject and for the exoskeleton are given in Table II. Fig. 6 shows an excellent fitting of the external vertical force F_Y and the moment along the lateral axis M_Z as measured by the WIIBB and as estimated using the identified dynamics model. Moreover, the estimated results using an anthropometric table (AT) [48] are also shown in Fig. 6. It can be seen that the F_Y and M_Z estimated using the identified parameter values are more accurate than those estimated using the AT. The average RMS differences of the identified F_Y and M_Z using the proposed method are respectively 0.26 ± 0.09 N/kg and 0.15 ± 0.08 Nm/kg (across all subjects), with respect to those measured using the WIIBB. Such differences show that the inertial parameters are well identified. The average RMS errors of the estimated F_Y and M_Z using the AT are 0.39 ± 0.11 N/kg and 0.28 ± 0.06 Nm/kg, respectively. Note that the motions that were requested to the subjects have been chosen to be feasible by the targeted patients. Moreover, if some parameters cannot be well excited, values identified using the AT method can be

TABLE II: Identified system's parameters

Parameters	Exoskeleton	Subject A	Subject B	Subject C	Subject D	Units
$m_{ei,hi}$	2.80, 4.18, 4.97	7.57, 15.58, 41.52	7.10, 14.52, 38.92	8.52, 18.07, 46.71	7.28, 15.43, 39.89	(kg)
$MX_i^{e,h}$	0.78, 1.50, 0.70	1.42, 3.98, 15.81	1.37, 3.86, 14.46	1.76, 4.91, 16.49	1.44, 4.14, 15.50	$(kg \cdot m)$
$I_{zi}^{e,h}$	0.22, 0.62, 0.50	0.76, 1.19, 7.24	0.78, 1.19, 6.39	1.03, 1.61, 9.67	0.52, 1.28, 8.57	$(kg \cdot m^2)$

$$MX_i^e = m_{ei} l_i k_{ei},\ MX_i^h = m_{hi} l_i k_{hi},\ I_{zi}^e = m_{ei}(l_i k_{ei})^2 + I_{ei},\ I_{zi}^h = m_{hi}(l_i k_{hi})^2 + I_{hi},\ \text{i} \in \{1,2,3\}$$

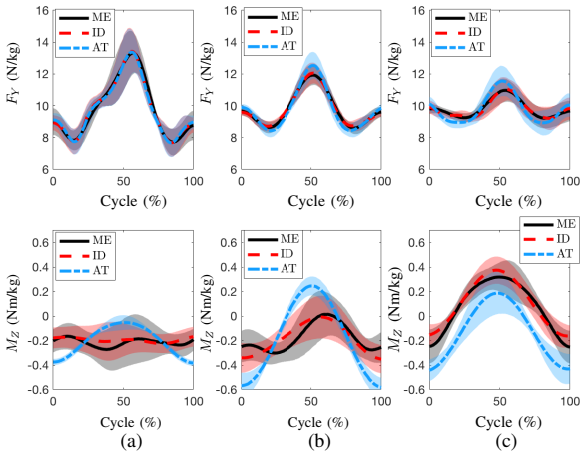


Fig. 6: Comparison of the external vertical forces (F_Y) and lateral moments of force M_Z measured by the WIIBB (ME) and estimated using the identified dynamic (ID) model and an anthropometric table (AT) [48] (across ten-time motions with Subject A). Gray zone shows the standard deviation. (a) squat motions, (b) oscillations of the hip/trunk, (c) oscillations of the ankle.

retained and the assistive ratios $\boldsymbol{\lambda}_1$ and $\boldsymbol{\lambda}_2$ need to be adjusted to satisfy the stability condition (39).

It should be noted that the parameters for the exoskeleton were only identified once with one subject. Since the lengths of the shanks and thighs of the exoskeleton were slightly adjusted (≤ 0.03m) for other subjects, the identified values of the first moments of inertia MX and the inertia I of these links were also adjusted by assuming the mass of the increase/decrease part of each link is zero. Since the masses of the shanks and thighs of the exoskeleton are low (see Table II), the modelling error caused using such a simplified method is very limited.

C. Simulation Study

To evaluate the effectiveness and robustness of the proposed impedance reduction control strategy, simulation studies were performed. Since the wearer's effort is taken into account during the STS movement, a simplified controller composed of an inverse-dynamic-model based feedforward part and a feedback proportional-derivative (PD) part is used to simulate the wearer's role [49]–[51]. Although a more complex human central-nervous-system like controller also includes other functions such as adaptive and stabilization abilities [49], a simplified controller can efficiently demonstrate the characteristics of the wearer's role and lead to intuitive insights into the performance of proposed impedance control strategy.

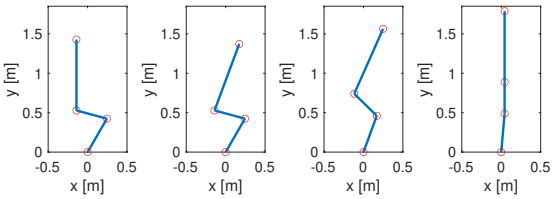


Fig. 7: Normal reference trajectory of the STS movement in simulation.

In addition, an alternative simplified method is used to directly detect the seat-off time rather than using the GRF (see eq.(4)), as follows:

$$\begin{cases} \beta_F = 1, & \text{if } \Delta h_{hip} \geq H_\beta \\ \beta_F = \frac{(\Delta h_{hip})^2}{H_\beta^2}, & \text{if } \Delta h_{hip} < H_\beta \end{cases} \tag{42}$$

where h_{hip} represents the increased vertical position of the hip joint, while H_β denotes a threshold after which the seat force completely converges to zero.

During the following simulations, the identified parameter values with the Subject A and the exoskeleton are used to build the human exoskeleton model (1) (see Table II). The PD parameter values are set as $K_p = 4000$ and $K_d = 300$. The parameter values related to the sliding mode-based controller (22) and the HJTO (15) are set as follows: $c_1 = 4$, $\sigma_s = 10$, $\lambda_s = 150$, $\sigma_1 = 50$, $\beta_o = 6$, $\zeta = 60$. *In the simulation, we assume that the exoskeleton is able to fully support the required torques for performing STS movements.*

1) Performance of Impedance Reduction: Firstly, the human-exoskeleton system is controlled using the PD and feedforwad controller (i.e., simulating the wearer) to track a normal STS reference trajectory which is designed based on healthy individuals' STS movements. Fig.7 shows the start, middle and end postures of human body according to the reference trajectory. The projected horizon position of the CoM (X_{CoM}) is assumed to be located at $-0.04 - 0.12$ m in front of the ankle joint during the STS movement. Hence, the virtual left and right margins of the X_{CoM} in equation (11) are set as -0.04 m and 0.12 m, respectively. To assess the impedance reduction of the proposed method, three simulations are performed with different STS periods (i.e., 3s, 5s, and 7s). According to the FTSTS test results [38], if the subject is able to perform a successful STS motion in $3s$, this means no external assistance is needed. Otherwise, longer STS times means weaker lower limb muscular ability. Given that, the parameter values related to the assistive ratios are chosen as $\delta_k = 0.8$, $\lambda_{k0} = 0.2$, $h_{th} = 1.211$, $\kappa_v = 1$, $v_{th} = 0.245$, $s_k = 4$ and $s_v = 19.6$. The parameter values related to

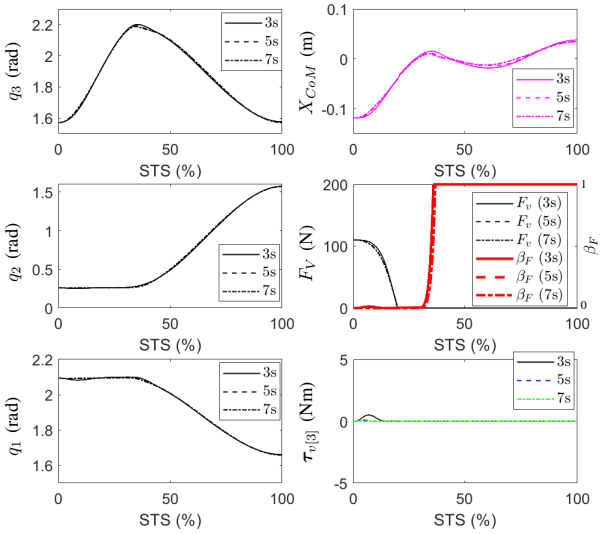


Fig. 8: Simulation results: STS movements with three different speeds (3s, 5s and 7s). q_1, q_2 and q_3 represent the ankle, knee and hip joint angles, respectively. X_{CoM} denotes the projected horizontal position of the CoM of the human-exoskeleton system. F_V is the virtual force, and $\boldsymbol{\tau}_{v[3]}$ is the virtual torque at the hip joint level. β_F is the GRF ratio.

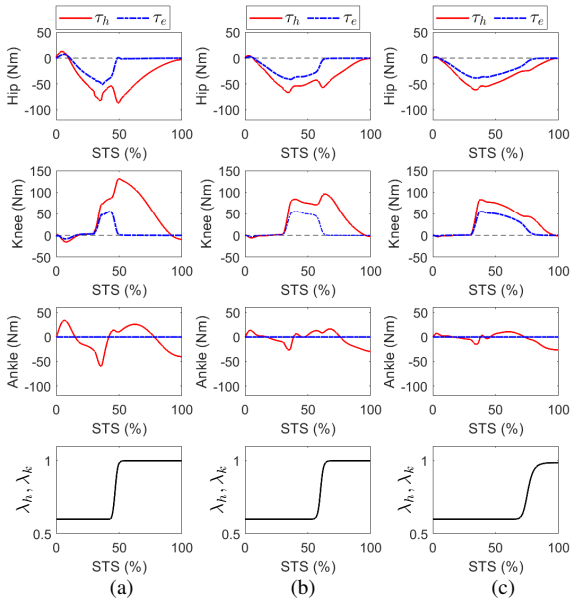


Fig. 9: Simulation results: performance of the impedance reduction during STS movements with three different speeds. a) STS in 3s, (b) STS in 5s, (c) STS in 7s. τ_h and τ_e show the human (PD and feedforward controller) joint torque and the assistive torque, respectively. λ_h and λ_k are the assistive ratios.

the virtual force are chosen as $F_{1max} = F_{2max} = 120$ and $K_{s1} = K_{s2} = 20$. Moreover, the wearer (the PD with feedforward controller) is assumed to be able to perform successful STS movements with the three different STS speeds.

Fig. 8 shows the normalized measured joint angles. During the three groups of STS movements, the wearer's joint trajectories are almost the same. The seat forces are set to converge to zero in the first 30% of each STS movement (see Fig.8). The measured X_{CoM} locates at $0.01 - 0.066$ m in front of the ankle joint after the GRF ratio β_F starts to increase to 1. From Fig.8 (F_v and β_F), the generated virtual torque $\boldsymbol{\tau}_{v[3]}$ is relatively low (< 1 Nm) and are also similar with the three groups of STS movements. However, significant differences in the wearer's torques (the output torques of the PD and feedforward controller) and the exoskeleton torques can be observed among the STS movements with the three speeds (see Fig.9). During the normal-speed STS movement (in 3s), the exoskeleton provides the wearer with only a short-time assistance at the beginning of the movement, while importance assistance is provided by the exoskeleton during the 7s STS movement to reduce the required human effort. In general, for performing the same STS movement with different speeds, the average ratios between the exoskeleton torques and the wearer's torques at the hip and knee joints level show both clearly increase with the STS times (see Fig. 9). In other words, the required torques for the wearer for achieving STS movements can be reduced to a desired level (see λ_h and λ_k in Fig. 9) according to the wearer's lower limb muscular ability.

In addition, the simulation results show that the tracking error for each joint using the designed SMC based controller can be limited to a very small range ($\|e_i\| < 0.002$ rad, $i \in 1, 2, 3$) (see Fig. 10). The estimation errors of the wearer's knee and hip joint torques during the normal-speed STS movement is relatively large but still limited into $\pm$ 20 Nm, while they can be significantly reduced during the 5s and 7s STSs (the root-mean-square (RMS) of $\tilde{\tau}_2$ and $\tilde{\tau}_3$ are respectively: 0.62 Nm and 1.21 Nm (5s), and 0.3 Nm and 0.67 Nm (7s)) (see Fig. 10). Note that a balance between the estimation accuracy and the noise reduction has been taken into account in the simulation.

Furthermore, a simulation study is carried out to compare the performances of the proposed HJTO and a commonly used method based on the inverse dynamic model and a Kalman filter. Joint angle trajectories measured with one subject during a STS movement are used as reference trajectories as shown in Fig.11. To estimate the joint torques, three methods are used: the inverse dynamic model with a zero-phase 2nd-order lowpass Butterworth filter, the inverse dynamic model with a Kalman filter and the designed HJTO with a 2nd-order lowpass Butterworth filter. For the first one, the measured joint angles are filtered using a zero-phase lowpass Butterworth filter at 2Hz. The joint velocities (accelerations) are calculated by numeric derivations of the joint angles (velocities). Then, the ankle, knee and hip joint torques are estimated using the inverse dynamic model. For the second one, a Kalman filter with a constant acceleration model [40] is used to estimate the joint angles, velocities and accelerations. Similarly, three joint torques are estimated using the inverse dynamic model. The covariances of the process and observation noises of three joints are set to be same and fine-tuned to ensure accurate estimation of the joint torques. For the last one, a lowpass

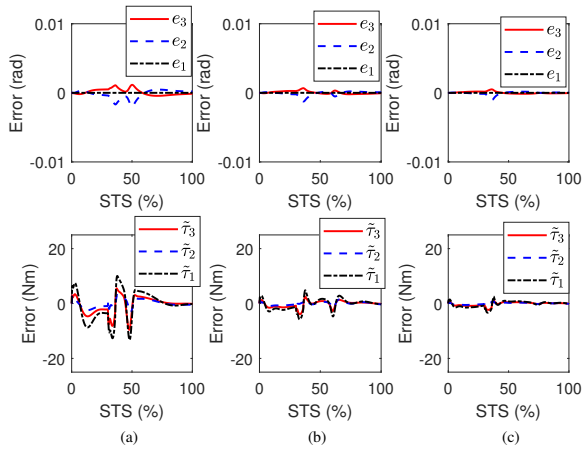


Fig. 10: Simulation results: tracking performance of the SMC-based controller and the estimation accuracy of the HJTO. (a) STS in 3s, (b) STS in 5s, (c) STS in 7s. e_1, e_2 and e_3 show the tracking errors of the ankle, knee and hip joint angles, respectively. $\tilde{\tau}_1$, $\tilde{\tau}_2$ and $\tilde{\tau}_3$ denote estimation errors of the ankle, knee and hip joint torques, respectively.

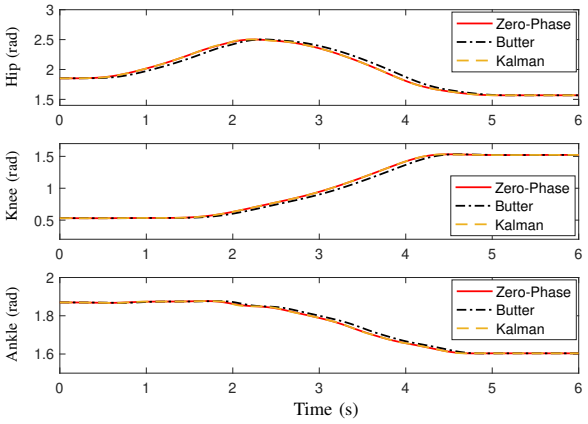


Fig. 11: Joint angles processed using three methods: a zero-phase lowpass Butterworth filter (Zero-Phase), a lowpass Butterworth filter (Butter) and a Kalman filter (Kalman).

Butterworth filter with a cutoff frequency of 2Hz is used to filter the measured joint angles. Then, the HJTO is used to estimate the three joint torques.

Fig. 12 shows the estimated joint torques using the three above-mentioned methods. Assuming that the joint torques estimated using the inverse dynamic model with the zero-phase lowpass filter are the real joint torques, one can notice that both the Kalman filter-based method and the HJTO one are able to ensure accurate joint torque estimations, while the Kalman filter-based one can further reduce the phase delay. However, when using the Kalman filter-based method in the proposed impedance reduction structure (see Fig. 4), the generated assistive torques may show significant differences from the wearer's joint torques (see Fig. 12(b)), while similar joint torque patterns can be guaranteed using the HJTO.

2) Robustness to System Modeling Uncertainties: To verify the robustness property shown in Section IV-C, a given mod-

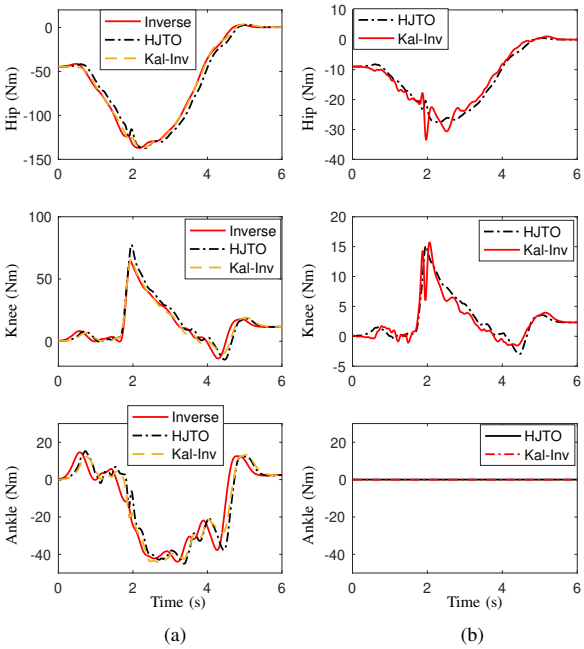


Fig. 12: Simulation results. (a) estimated joint torques using three methods: the inverse dynamic model with a zero-phase lowpass Butterworth filter (Inverse), the inverse dynamic model with a Kalman filter (Kal-Inv) and the HJTO with a lowpass Butterworth filter, (b) generated assistive joint torques based on the HJTO and the inverse dynamic model with a Kalman filter.

elling uncertainty ($\boldsymbol{M} = 1.5\boldsymbol{M}^*$, $\boldsymbol{C} = 1.5\boldsymbol{C}^*$, $\boldsymbol{G} = 1.5\boldsymbol{G}^*$) is introduced in the human-exoskeleton model. The time-varying assistive ratio (8) is similar to the one used in Section V-C1, except for the values of the parameters δ_k and λ_{k0}, which are given in the following. In addition, smaller PD gains ($K_p = 4000$ and $K_d = 120$) are used to simulate the performance of the wearer under stable and unstable states.

Comparison simulations were respectively performed under the following five conditions: (a) Constant assistive ratios, $\lambda_h = \lambda_k = 0.8$; (b) Constant assistive ratios, $\lambda_h = \lambda_k = 0.65$; (c) Designed time-varying assistive ratios with $\delta_k = 0.825$, $\lambda_{k0} = 0.175$; (d) Designed time-varying assistive ratios with $\delta_k = 0.75$, $\lambda_{k0} = 0.25$; (e) Designed time-varying assistive ratios with $\delta_k = 0.65$, $\lambda_{k0} = 0.35$.

Fig. 13 shows the simulation results. According to the stability condition (39), the assistive torques $\boldsymbol{\tau}_e$ should be stable under the first four conditions. However, chatterings can be observed in both the assistive torques $\boldsymbol{\tau}_e$ and the human torques $\boldsymbol{\tau}_h$ when the wearer's posture is close to the standing posture under the condition (b). This is due to the fact that the large reduction of the desired impedance, particularly the desired inertia, makes the designed PD gains no longer suitable, i.e., the PD gains should be re-tuned. According to equation (37), the real desired impedance under the conditions (a) and (b) are only 46.7% and 29.2% of the nominal ones, respectively. Although human has the capability of stabilizing a stable/unstable system by optimizing joint impedance [49]–

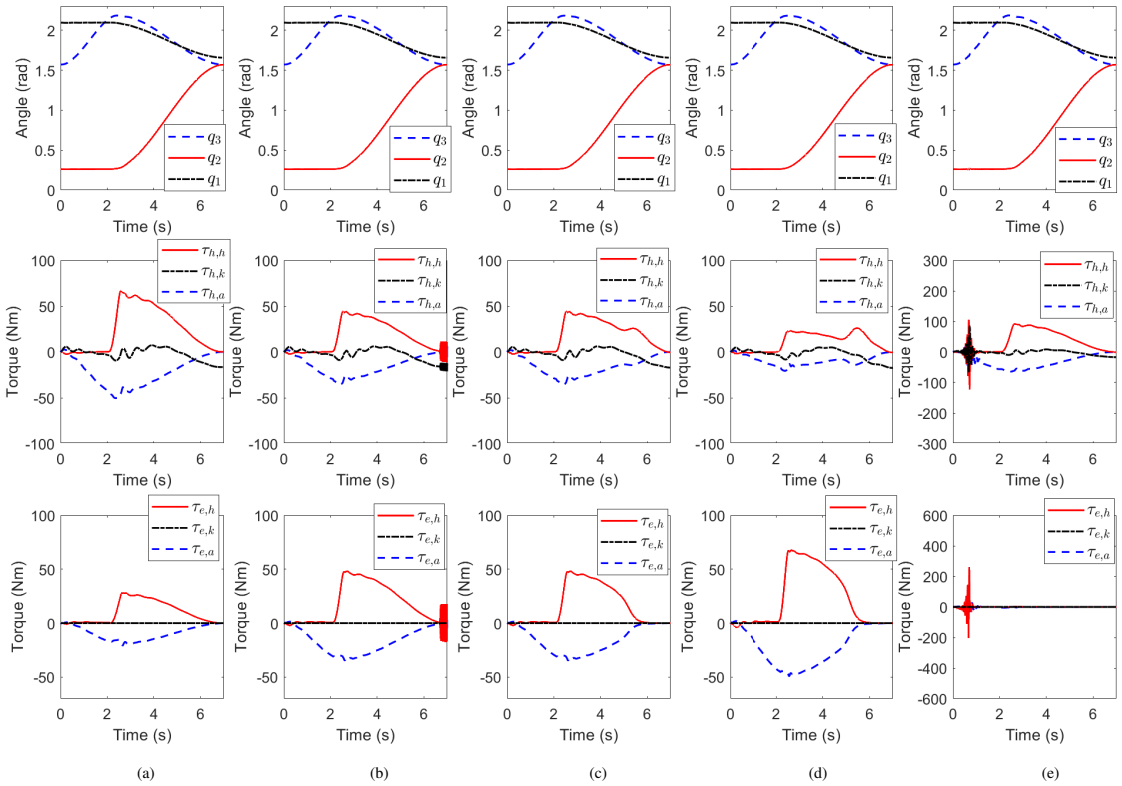


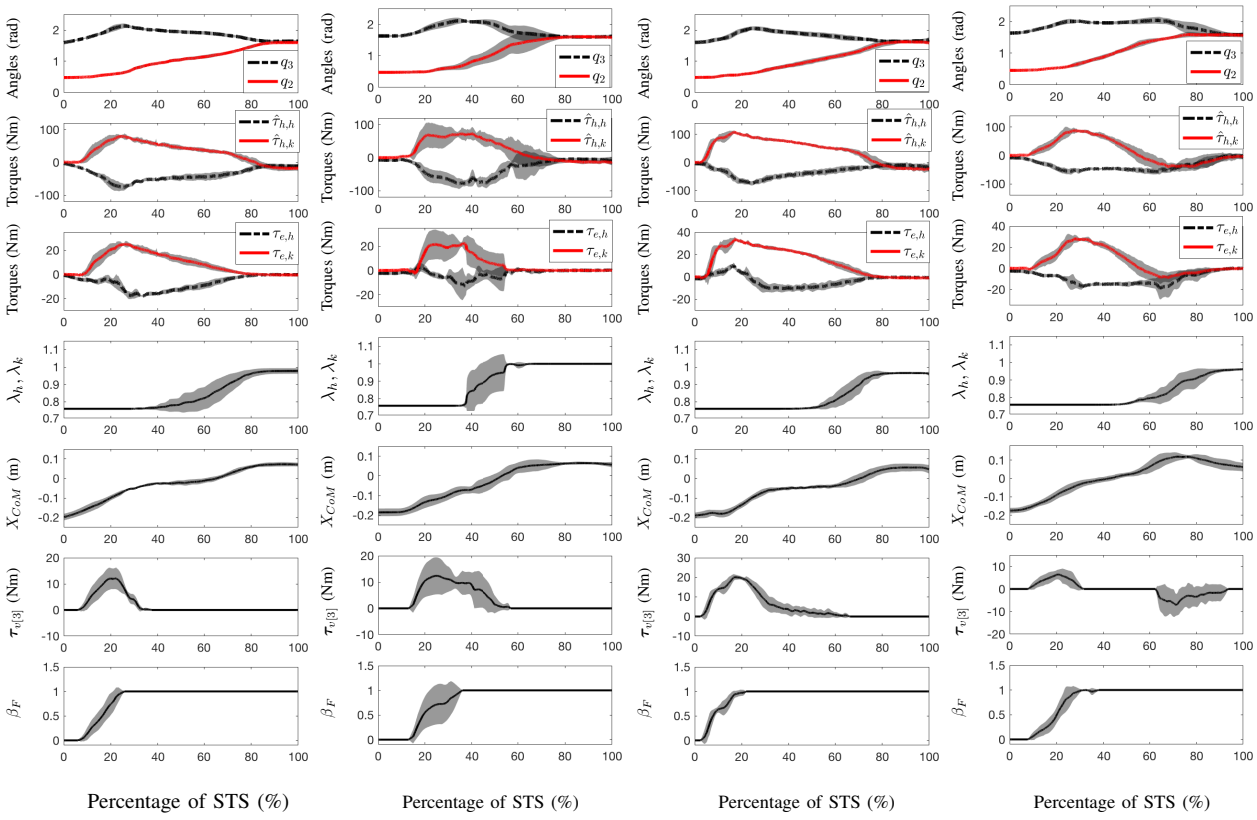
Fig. 13: Robustness with respect to modeling uncertainties. The system norminal model is set as $\boldsymbol{M} = 1.5\boldsymbol{M}^*$, $\boldsymbol{C} = 1.5\boldsymbol{C}^*$, $\boldsymbol{G} = 1.5\boldsymbol{G}^*$. (a) constant assistive ratios are $\lambda_h = \lambda_k = 0.8$. (b) constant assistive ratios are $\lambda_h = \lambda_k = 0.65$. (c) designed time-varying assistive ratios with $\delta_k = 0.825$, $\lambda_{k0} = 0.175$. (d) designed time-varying assistive ratios with $\delta_k = 0.75$, $\lambda_{k0} = 0.25$. (e) designed time-varying assistive ratios with $\delta_k = 0.65$, $\lambda_{k0} = 0.35$. q_1, q_2 and q_3 show the ankle, knee and hip joint angles, respectively. τ_h and τ_e represent human torque and the assistive torque, respectively. Subscripts a, k and h denote the ankle, knee and hip joints, respectively.

[51], it is difficult for the wearer to cope with the large chattering during standing posture (see Section V-D3), especially for individuals with muscular weaknesses. On the other hand, the chattering effect can be effectively compensated using the proposed time-varying assistive ratio function (condition (c)), which ensures increasing in the assistive ratio when the wearer is close to the standing posture (see Fig. 13(c)). The proposed function ensures, at the same time, significant assistance to the wearer during the main power-demanding part of the STS movement. Furthermore, it can be seen that a further smaller assistive ratio can be used with the designed time-varying ratio function to gain higher assistance without causing the chattering problem (see Fig. 13(d)). Under the condition (e), the closed-loop human-exoskeleton becomes unstable at the beginning of the STS since the stability condition (39) cannot be satisfied. In addition, a transient large vertical velocity of the wearer's HAT CoM v_{max} is caused due to the chattering effect and the assistive ratios increase to 1.

D. Experimental evaluation

1) Assistive performance during four types of STS strategies: The main goal of the proposed method is to reduce the required wearer's effect for achieving a successful STS movement. The torque assistive performance of the proposed method was investigated in detail during four types of STS strategies, including *normal STS strategies with two different speeds (low speed (in 15s) and medium speed (in 8s)) and two abnormal STS strategies which may cause sitback and step, respectively*. Low- and medium-speed STS movements are commonly observed in the populations with lower-limb muscular weakness [38]. In addition, sitback and step, which are the two typical modes of most STS failures observed in the elderly, both result from muscular weakness and/or lack of balance control and motion coordination [3]. Note that performing a STS movement in an abnormal way, i.e., sitback-like or step-like movements, may require even larger human joint torques at one or two specific joint levels, which further increases the risk of STS failures.

Four healthy subjects participated in the experiments under two conditions: "in exoskeleton with assistance (WA)" and "in exoskeleton without assistance (WOA)". For each type of STS strategies, each subject was asked to separately and alternatively carry out three groups of FTSTSs under two conditions, with a 5-minute rest in-between. Meanwhile, at least 20-minute break was taken between the achievements of the different types of STS motions, and a 15-second rest



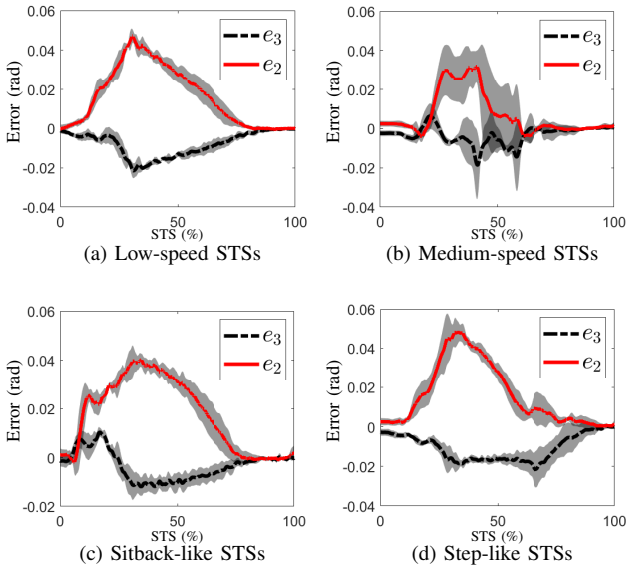
(a) Low-speed STSs (b) Medium-speed STSs (c) Sitback-like STSs (d) Step-like STSs

Fig. 14: Experimental results with one subject (on average, across five STS movements) during four types of STS strategies such as low-speed, medium-speed, sitback-like and step-like. The wearer's kinematic and kinetic data and the outputs of each part of the proposed method are presented. q_3 and q_2 show the hip and knee joint angles, respectively. $\hat{\tau}_{h,h}$ and $\hat{\tau}_{h,k}$ are the estimated human hip and knee joint torques, respectively. $\tau_{e,h}$ and $\tau_{e,k}$ are the assistive hip and knee joint torques, respectively. λ_h and λ_k are the assistive ratios. X_{CoM} denotes the horizontal position of the CoM of the human-exoskeleton system. $\boldsymbol{\tau}_v[3]$ is the virtual torque, and β_F the GRF ratio. Gray zone shows the standard deviation.

was imposed between two continuous STS motions during one group of FTSTSs. To mimic the state of people with lower-limb muscular weakness, one subject (Subject A) was also asked to run on a treadmill with a speed of 9Km/h for 10 minutes, and then to perform the STS movements with significant lower-limb muscular fatigue. In other words, Subject A did twice experiments under two different states: without and with muscular fatigue. Here, Subject A* indicates Subject A in the state of lower-limb muscular fatigue.

To perform STS movements at the given speeds, a timer was used as a sound reference to help the subjects controlling their speeds. Note that the stand-to-sit movements were not assisted. During the medium-speed STS motions, the subject was asked to stand up from a chair slowly at the early power-demanding phase, and then, extend the hips and knees with a normal speed (see Fig. 14(b)). During the sitback-like STS movements, each subject was asked to sit on a chair while keeping the torso in the vertical direction, and then, standing up directly without a prior forward bending of the torso (see Fig. 14(c)). In this case, significant human knee torques are required to shift the CoM of the human-exoskeleton forward. During the step-like STS movements, each subject was asked to first flex the hip joint to around 60 degrees during sitting position, and then, standing up without extending the hip joints until the knee joints were sufficiently extended. In this case, the X_{CoM} of the human-exoskeleton is then over 0.1 m in front of the ankle joint (see Fig. 14(d)), and the subject is close to loose the balance.

Due to the limitation of the maximum output torques of the exoskeleton actuators, the range of assistive ratio (8), i.e., $[\delta_k - \lambda_{k0},\ \delta_k + \lambda_{k0}]$), was designed for each subject to take full advantage of the exoskeleton assistance, as follows: [0.75 1] (Subjects A and A*), [0.85 1] (Subject B), [0.76 1] (Subject C), [0.78 1] (Subject D). In addition, the margins (x_{c1}, x_{c1}) of virtual torques were also slightly adjusted for each subject according to their heights as follows: (-0.04 0.12) for Subjects A, A*, B and D) and (-0.02 0.1) for Subject C. The value of the HJTO parameter σ_1 was set for each subject based on the



(a) Low-speed STSs (b) Medium-speed STSs

(c) Sitback-like STSs (d) Step-like STSs

Fig. 15: SMC tracking errors with one subject (on average, across 5 STS movements) during four types of STS strategies. e_3 and e_2 show the hip and knee joint tracking errors, respectively. Gray zone shows the standard deviation.

TABLE III: Experimental Parameter Settings

Eq.s	Parameters	Values
(8), (10)	s_k, s_v, v_{th}, κ_v	4, 19.6, 0.245, 1
(11)	K_{s1}, K_{s2}, F_{1max}, F_{2max}	20, 30, 60, 120
(19)	β_o, ζ	50, 6
(22)	c_1, σ_s, λ_s	4, 10, 120

condition (20): 25, 30, 22 and 30 (Subjects A, B, C and D, respectively). The values of the remaining parameters related to the proposed impedance modulation method are given in Table III.

To assess the assistive effectiveness of the proposed method, five EMG sensors (Delsys, USA) were used to record the related muscles' activities. EMG signals corresponding to the activities of the vastus lateralis (VL) and biceps femoris (BF) muscles of each leg and the erector spinae muscle (ES) in the lumbar region are compared to show the assistive effects of the proposed method at the knee and hip (torso) joints level under the two designed conditions. The EMG signals were sampled at 150 Hz. The raw EMG signals were processed as follows: highpass filtered at 10Hz using a zero-phase fourth-order Butterworth filter; rectified; low pass filtered at 4Hz using a zero-phase fourth-order Butterworth filter.

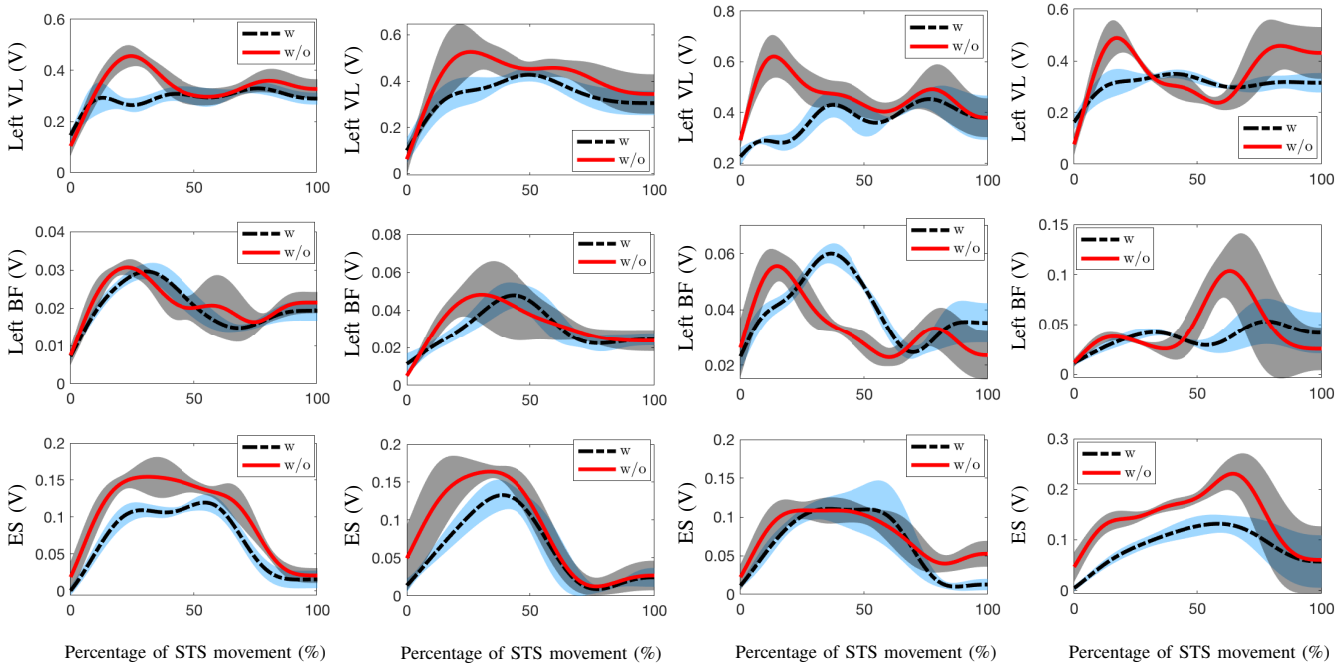
For each type of STS strategies, experimental results obtained during five representative STS movements under each condition are selected. Student's t-test is used to ensure there is no difference in the STS time between the selected STS movements under the two conditions. Here, the STS time is defined as the period from the beginning of the knee joint extension to the end of the STS movement, in which the VL, BF and ES muscles are mainly activated.

Fig. 14 shows the experimental results (on average, across five STS movements) with one subject (Subject A) under the condition WA during the four types of STS strategies. In general, the assistive hip/knee joint torques $\tau_{e,h}$ and $\tau_{e,k}$ show similar profiles as those of the estimated human joint torques $\hat{\tau}_{h,h}$ and $\hat{\tau}_{h,k}$ during all STS movements, except for the parts affected by the reduction of the impedance ratios λ_h and λ_k as well as the virtual torque $\tau_{v[3]}$.

During the low-speed STS movements, the assitive ratios λ_h and λ_k are relatively small during the early and middle phases of the STS movement and increase gradually to 1 with the increase of the height of the CoM of the wearer's HAT, h_{hHAT}. Correspondingly, important assistive torques are provided to the wearer's hip and knee joints to reduce the wearer's muscle efforts during the low-speed STS motions (see Fig. 14 (a)). Similarly, significant assistive torques are provided during the main torque-demanding period of the sitback-like and step-like STS movements since their speeds are also relatively low (see Fig. 14 (c) and (d)). On the other hand, the assistive torque is mainly provided at the early phase of the medium-speed STS movements, and then, quickly decreases to zero when the subject stands-up with a high speed (see Fig. 14(b)). It can be seen that high joint torques are still required from the wearer to achieve the STS movements after the assistive torques largely reduce. It is assumed that wearer needs no extra assistance (i.e., no lower-limb muscular weakness) if he/she can quickly stand up from a chair [38].

A virtual torque is applied at the early phase of each type of STS strategies, as shown in Fig. 14. It firstly increases with the GRF ratio β_F, and then, fades to zero when the horizontal position of the CoM of the human-exoskeleton system, X_{CoM}, is approaching the designed left margin -0.04m. During the low- and medium-speed STS movements, the virtual torque during the initial phase can partially counteract the assistive hip joint torque caused by the impedance reduction (12) (see Fig. 14(a) and (b)). This is due to fact the wearer synchronously flexes the hips and extends the knees during the initial phases of these STS movements. In this case, the use of the virtual torque ensures that the wearer would be able to easily flex the hips during the initial phases of the low- and medium-speed STS movements. Note that the assistive hip joint torque should show a similar profile to the estimated hip joint torque without the virtual torque.

During the sitback-like STS movements, the subject starts rising from the chair before bending the HAT (see the β_F and q_3 in Fig. 14(c)), then, a large virtual torque is triggered according to equations (11) and (13). Correspondingly, a positive hip joint torque is generated to flex the hip joints to move the CoM of the wearer and exoskeleton forward during the early phase of the STS movement. During the step-like STS movements, virtual torques are generated during both early and late phases, as shown in Fig. 14(d). Since the early phase of step-like STS movement is similar to the one of low-speed motions, a virtual torque is also generated to ensure that the wearer is able to easily bend the HAT. During the late phase of the step-like STS movement, a virtual torque is generated when the X_{CoM} moves far away from the ankle joint. As a result, an extra torque is added to the assistive hip joint torque $\tau_{e,h}$ to assist the wearer to extend the



(a) Low-speed STSs (b) Medium-speed STSs (c) Sitback-like STSs (d) Step-like STSs

Fig. 16: EMG patterns for one subject during four types of STS strategies under two conditions (on average, across five STS movements). w and w/o represent "in exoskeleton without assistance" and "in exoskeleton with assistance", respectively. Gray zone shows the standard deviation.

hip joints and move the X_{CoM} back to the designed range, $[-0.04 \quad 0.12]$m.

As mentioned in Section IV, the performances of the SMC and HJTO are important for achieving the desired impedance model. Fig. 15 shows the average tracking errors $\boldsymbol{e}_2$ and $\boldsymbol{e}_3$ obtained with the proposed SMC controller with a representative subject (Subject A) during four types of STS strategies. Although the tracking errors increase with the joint velocities, they can be limited to a small range. The average RMSs of the $\boldsymbol{e}_2$ and $\boldsymbol{e}_3$ across all STS motions are 0.01 ± 0.003 rad and 0.021 ± 0.004 rad, respectively. Such accuracy satisfies the condition to accurately track the desired trajectory generated from the desired impedance model. During the experiments, it can be observed that the assistive joint torques, particularly the knee joint torque, show similar profiles as those of the estimated wearer's joint torques, without being influenced by the changes of the impedance ratios and the virtual torques (see Fig. 14).

2) EMG reduction: The EMG signals measured from VL and BF muscles of both legs and the ES muscle are compared to show the impact on the wearer's muscle effort under two conditions WOA and WA. Fig. 16 shows the EMG patterns for a representative subject (Subject A) during four types of STS strategies under the two conditions (on average, across five STS movements). Since the left and right VL/BF muscles deliver similar torques during the STS movements, only the EMG patterns of the left VL/BF muscles are shown. The average STS time of each subject under the two conditions are shown in Fig. 17. For each subject and each type of STS strategies, there is no significant difference ($p > 0.2$, t-test) between the STS time under the two experimental conditions.

During the early torque demanding phase of the low-speed STS movement, the VL muscle effect is largely reduced in condition WA compared to condition WOA. Meanwhile, the ES muscle effort is reduced for this subject during the whole period of the low-speed STS movement in condition WA (see Fig. 16(a)). During the early and middle phases of the medium-speed STS movement, a similar reduction in the VL and ES muscles' effects can be observed in condition WA (see Fig. 16(b)). However, there is no notable difference in the ES muscle effect in the late phase of the medium-speed STS movements between the two conditions due to the reduction in the assistive torque (see Fig. 14(b)) in condition WA. By comparing the muscular activities during the early phase of the low-speed STS movements in condition WOA, the VL muscle is more activated during the early phase of the sitback-like STS movements in the same condition. However, the VL muscle effect can be remarkably decreased during the early phase of the sitback-like STS movements in condition WA (see Fig. 16(c)). During the middle/late phases of step-like STS movements, important ES muscle activity is required in condition WOA (see Fig.16(d)). On the other hand, it can be seen that the ES muscle activity is largely reduced in condition WA. Meanwhile, the VL muscle activity is also reduced during the early phase of the step-like STS movement. With regard to

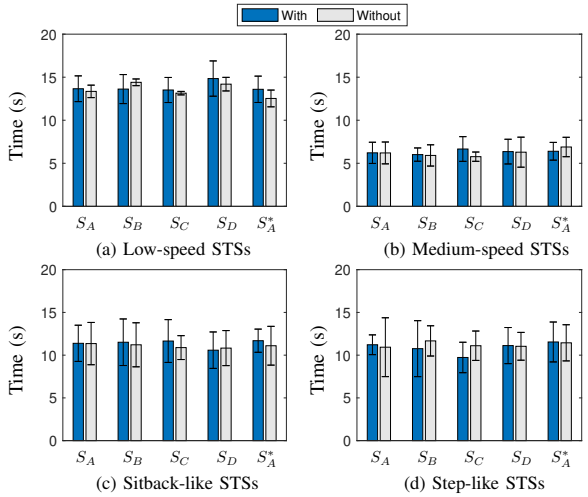


Fig. 17: Average STS time of each subject during four types of STS strategies under two conditions (with and without assistances). S_i denotes Subject i, $i \in \{A, B, C, D, A^*\}$.

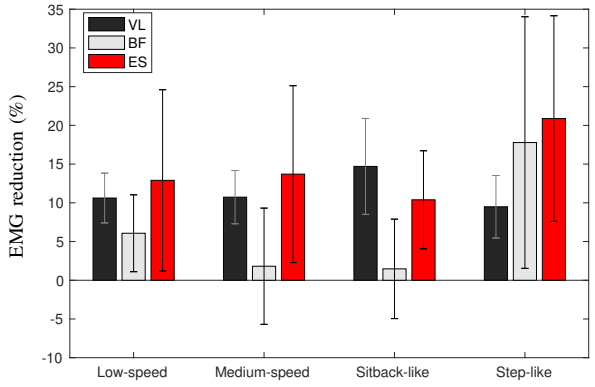


Fig. 18: Average reduction of the RMS of the processed EMG signals across all subjects during four types of STS strategies. VL and BF denote the average reduction of left and right VL and BF muscles, respectively.

the BF muscle, it shows relative low activities during the low-speed, medium-speed and sitback-like STS movements while no notable muscular co-contraction is observed during these STS movements. During the late phase of the step-like STS movement, the BF muscle is more activated to shift the CoM of the human exoskeleton system back in condition WOA. However, such BF muscle effect is not needed in condition WA since the exoskeleton assistance can prevent the CoM of the human exoskeleton system from moving too far from the ankle joint.

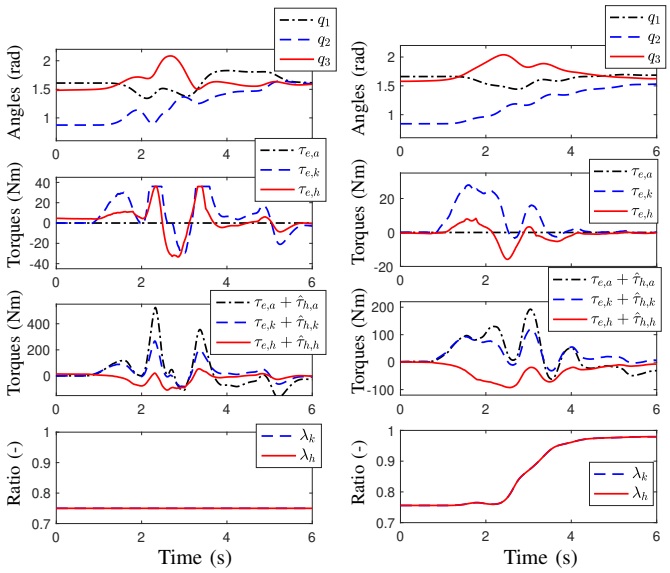
Due to the variability of subjects' motions and musculoskeletal systems, it is inevitable that there exist some differences in the EMG signals across all subjects. Fig. 18 shows the average reductions of the RMS of the processed EMG signals across all subjects during four types of STS strategies in condition WA, compared to condition WOA. For sake of simplicity, the average reductions achieved for the left and right VL/BF muscles are presented instead of showing both

TABLE IV: EMG reduction across all subjects under different conditions. S_i denotes Subject i, $i \in \{A, B, C, D, A^*\}$.

Muscles	S_A	S_B	S_C	S_D	$S_A{}^*$	Average
	Low-speed STSs (unit:%)					
Mean VL	10.87	14.72	5.71	10.51	11.27	10.6±3.2
Mean BF	0.96	7.43	9.99	11.25	0.74	6.1±5.0
ES	30.70	6.70	18.04	0.93	8.12	12.9±11.7
	Medium-speed STSs (unit:%)					
Mean VL	13.92	10.34	5.27	10.73	13.39	10.7±3.4
Mean BF	-3.78	1.23	1.05	13.74	-5.19	1.8±7.5
ES	20.19	4.69	16.53	-0.41	27.52	13.7±14.2
	Sitback-like STSs (unit:%)					
Mean VL	21.45	8.57	12.06	10.18	21.25	14.7±6.2
Mean BF	-5.13	8.04	-0.40	8.46	-3.61	1.5±6.4
ES	2.96	13.92	16.69	4.18	14.19	10.4±6.3
	Step-like STSs (unit:%)					
Mean VL	10.29	5.55	13.78	5.04	12.78	9.5±4.0
Mean BF	45.46	13.93	16.96	8.51	4.06	17.8±16.2
ES	40.90	9.01	11.81	15.00	27.69	20.9±13.3

sides. During the low-speed STS movements, the VL and ES muscle activities are reduced by $10.6 \pm 3.2\%$ and $12.9 \pm 11.7\%$, respectively. Similar reductions (VLs: $10.7 \pm 3.4\%$; ES: $13.7 \pm 14.2\%$) can also be observed during the medium-speed STS movements. The VL muscle activities are further reduced ($14.7 \pm 6.2\%$) during the sitback-like STS movements, while less reduction ($9.5 \pm 4.0\%$) are observed during the step-like STS movements. On the contrary, the EMG signals measured from ES muscle are further reduced ($20.9 \pm 13.3\%$) during the step-like STS movements, while less reduction ($10.4 \pm 6.3\%$) is observed during the sitback-like movements. This means that the assistive torque induced by the virtual torque can further assist in reducing the corresponding muscular activities to avoid failures in sitback-like or step-like STS movements. There is no significant decrease in the BF muscles' EMG signals between WA and WOA conditions during the medium-speed STSs ($1.8 \pm 7.5\%$; $p = 0.69$, t-test) and the sitback-like STSs ($1.5 \pm 6.4\%$; $p = 0.64$, t-test). The reduction of the BF muscles' EMG signals is also relatively low ($6.1 \pm 5.0\%$) during the low-speed STS movements. It should be noted that the contraction level of the BF during these three STS movements is very limited (see Fig. 16). However, a large reduction in the BF muscles' EMG signals can be observed ($17.8 \pm 16.2\%$) during the step-like STS movements due to the fact that important BF muscle contraction is needed to maintain balance during the late phase of this type of STS movements in condition WOA. Detailed EMG reduction percentages for each subject are given in Table IV. Since the HAT of Subject D is much higher than the one of the exoskeleton (0.89m *vs* 0.31m), the assistive effectiveness for HAT extension is not notable (average ES reduction = $1.6 \pm 2.4\%$) during the low-speed, medium-speed and sitback-like STS movements.

During the experiments, subject A* was asked to keep a similar squat posture for five seconds before and after running on the treadmill. Meanwhile, the EMG signal of left VL muscle was recorded to show the VL muscle fatigue state. The obtained results show that the mean frequency of the power spectral density of the measured VL muscle EMG signals is decreased by 8.6% and that the VL muscle is relatively



(a) (b)

Fig. 19: Robustness study: (a) using a constant assistive ratio, $\lambda_h = \lambda_k = 0.6$, (b) using the developed assistive ratio function. q_1, q_2 and q_3 show the ankle, knee and hip joint angles, respectively. $\hat{\tau}_h$ and τ_e represent the estimated wearer's joint torques and the assistive torques, respectively. The second subscript a, k and h denote the ankle, knee and hip joints, respectively.

fatigued after 10-minute fast running, according to the method presented in [52]. One can notice significant reductions in the EMG signals measured from the VL muscles ($14.7 \pm 4.5\%$; $p = 0.007$, t-test) and ES muscle ($19.4 \pm 9.8\%$; $p = 0.03$, t-test) of Subject A* across all types of STS strategies in condition WA, compared to condition WOA. This shows that the proposed impedance modulation control strategy has the potential to effectively reduce the muscular activities of subjects with muscular weaknesses to perform successful STS movements.

3) Robustness evaluation: A comparison experiment was carried out to demonstrate the robustness of the proposed control strategy with respect to the chattering effect during the end phase of the STS movements. Subject A participated in this experiment and a modeling error was added to the nominal model, i.e., $\boldsymbol{M} = 1.3\boldsymbol{M}^*$, $\boldsymbol{C} = 1.3\boldsymbol{C}^*$, $\boldsymbol{G} = 1.3\boldsymbol{G}^*$. The parameter λ_{k0} and δ_k were set to 0.2 and 0.8, respectively. Due to the limitation of the maximum output torque of the exoskeleton actuators, a relatively high chair (0.7m) was used. The subject was asked to stand up from the chair with the assistance of the exoskeleton under two conditions: 1) using a constant assistive ratio, $\lambda_h = \lambda_k = 0.6$; 2) using the proposed assistive ratio function (8).

Under the first condition, large chattering occurs in the joint angles (see Fig. 19(a)), and results in a significant increase in the wearer's joint torques and the saturation of the assistive torques. Due to the modelling error, the real coupled impedance of the human-exoskeleton system is much lower than the desired one. Hence, fast motions can be caused by a relatively small joint torque when the wearer's posture is close to the standing posture, particularly when the knee joint angle crosses the zero. Once a chattering occurs, significant wearer's joint torque/impedance is needed to stabilize the system. This increases the fall risks of subjects suffering from muscular weaknesses. Under the second condition, however, the chattering effect can be compensated using the proposed assistive ratio function (see Fig. 19(b)). The assistive ratio was increased with the height of the wearer's HAT CoM as well as the standing speed so that the coupled real impedance of the human-exoskeleton system can also increase. Note that stability of the human-exoskeleton system is not only determined by the coupled real impedance of the human-exoskeleton system, but also by the subject's control ability (37).

VI. Conclusion

In this article, an impedance modulation control strategy of a lower limb exoskeleton was proposed to assist dependent people to achieve successful sit-to-stand movements. The potential users are supposed to have a certain lower limb motion ability, but not sufficient to achieve a successful STS movement. In this case, an impedance compensation assistance of the exoskeleton was designed to reduce the mechanical impedance of the human-exoskeleton system to a lower level than the wearer's motor ability. Moreover, a balance reinforcement assistance was developed to avoid two typical failed STSs, "sit-back" and "step", due to balance loss. These two assistance functions were both addressed using a desired impedance model. To adapt the human-exoskeleton model to the proposed desired one, a practical human joint torque observer was proposed to estimate the wearer's joint torques; a time-varying desired impedance model was proposed based on the wearer's motor ability; a high gain controller was used to provide sufficient power support to accomplish the active impedance assistance. Furthermore, the characteristics and robustness of the proposed methods were theoretically analyzed and discussed. Since the proposed control strategy is model-based, a system identification algorithm was used to ensure accurate system modelling. Finally, the effectiveness of the proposed methods was evaluated via simulations and experiments. The results show that the proposed impedance modulation control strategy can efficiently reduce the human-exoskeleton impedance, and provide appropriate power support to the wearer for both human effort reduction and balance reinforcement. In future work, a new lower-limb exoskeleton will be deigned for providing higher assistive torques to the wearer. Meanwhile, further studies will be carried out to investigate subjects' control abilities during STS movements with respect to different assistive ratios.

APPENDIX A
MODELING OF THE SIT-TO-STAND MOVEMENT

The matrices $\boldsymbol{J}_\Theta$ and $\boldsymbol{J}_F$ in (1) are shown as follows:

$$\boldsymbol{J}_\Theta = \begin{bmatrix} 1 & 0 & 0 \\ 1 & 1 & 0 \\ 1 & 1 & 1 \end{bmatrix}, \quad \boldsymbol{J}_F = \begin{bmatrix} l_1 s_1 & l_2 s_2 & 0 \\ l_1 c_1 & l_2 c_2 & 0 \end{bmatrix}. \tag{43}$$

The matrix $\boldsymbol{H}$ in (5) is given as follows:

$$\boldsymbol{H} = \begin{bmatrix} 1 & 0 & 0 \\ 0 & 1 & 0 \end{bmatrix}. \tag{44}$$

APPENDIX B
ANALYSIS OF THE TRACKING PERFORMANCE

Proof. Consider the following candidate Lyapunov Function:

$$\boldsymbol{V} = \frac{1}{2}\boldsymbol{s}^T \boldsymbol{M}(\boldsymbol{q})\boldsymbol{s}. \tag{45}$$

By differentiating both sides of (45), we obtain:

$$\dot{\boldsymbol{V}} = \boldsymbol{s}^T \boldsymbol{M}(\boldsymbol{q})\dot{\boldsymbol{s}} + \frac{1}{2}\boldsymbol{s}^T \dot{\boldsymbol{M}}(\boldsymbol{q})\boldsymbol{s}. \tag{46}$$

Since $\dot{\boldsymbol{M}}(\boldsymbol{q}) - 2\boldsymbol{C}(\boldsymbol{q}, \dot{\boldsymbol{q}})$ is skew-symmetric, we have:

$$\boldsymbol{s}^T[\dot{\boldsymbol{M}}(\boldsymbol{q}) - 2\boldsymbol{C}(\boldsymbol{q}, \dot{\boldsymbol{q}})]\boldsymbol{s} = \boldsymbol{0}. \tag{47}$$

From (1), (47), (12), and (22), equation (46) can be expressed as follows:

$$\begin{aligned}
\dot{\boldsymbol{V}} &= \boldsymbol{s}^T \boldsymbol{M}(\boldsymbol{q})\dot{\boldsymbol{s}} + \boldsymbol{s}^T \boldsymbol{C}(\boldsymbol{q}, \dot{\boldsymbol{q}})\boldsymbol{s} \\
&= \boldsymbol{s}^T(\boldsymbol{M}(\boldsymbol{q})c_1\dot{\boldsymbol{e}} + \boldsymbol{M}(\boldsymbol{q})\ddot{\boldsymbol{e}} + \boldsymbol{C}(\boldsymbol{q}, \dot{\boldsymbol{q}})\boldsymbol{s}) \\
&= \boldsymbol{s}^T(\boldsymbol{M}(\boldsymbol{q})c_1\dot{\boldsymbol{e}} + \boldsymbol{M}(\boldsymbol{q})\ddot{\boldsymbol{q}} - \boldsymbol{M}(\boldsymbol{q})\ddot{\boldsymbol{q}}_r + \boldsymbol{C}(\boldsymbol{q}, \dot{\boldsymbol{q}})\boldsymbol{s}) \\
&= \boldsymbol{s}^T(\boldsymbol{M}(\boldsymbol{q})c_1\dot{\boldsymbol{e}} + \boldsymbol{U}_h + \boldsymbol{U}_e + \boldsymbol{J}_F^T\boldsymbol{F} - \boldsymbol{G}(\boldsymbol{q}) \\
&\quad - \boldsymbol{C}(\boldsymbol{q}, \dot{\boldsymbol{q}})\dot{\boldsymbol{q}} - \boldsymbol{M}(\boldsymbol{q})\ddot{\boldsymbol{q}}_r + \boldsymbol{C}(\boldsymbol{q}, \dot{\boldsymbol{q}})\boldsymbol{s}) \\
&= \boldsymbol{s}^T(\boldsymbol{U}_h - \hat{\boldsymbol{U}}_h - \boldsymbol{R}\boldsymbol{\tau}_v - \sigma_s \text{sat}(\boldsymbol{s}) - \lambda_s \boldsymbol{s}) \\
&= \boldsymbol{s}^T(\tilde{\boldsymbol{U}}_h - \boldsymbol{R}\boldsymbol{\tau}_v - \sigma_s \text{sat}(\boldsymbol{s}) - \lambda_s \boldsymbol{s}) \leq 0.
\end{aligned}$$

Therefore, the Lyapunov function is decreasing. This completes the proof. Note that σ_s can be set to a smaller value, $0 < \sigma_s < \frac{2\varepsilon\sigma_1\|\boldsymbol{X}\|^2}{\eta\Gamma}$, in practice, to avoid the chattering effect in the control torque. In this case, the tracking error $\boldsymbol{s}$ can converge into a range $\|\boldsymbol{s}\| < \frac{\varepsilon_v}{\lambda_s}$, which can be easily proved according to the aforementioned proof.

APPENDIX C
ROBUSTNESS WITH RESPECT TO MODELING UNCERTAINTIES

Proof. Here we only investigate the situation where there is no torque applied by the wearer and the trajectory tracking control has converged. The desired impedance model (37) can therefore be represented by:

$$\boldsymbol{\lambda}_1(\boldsymbol{M}(\boldsymbol{q}_r)\ddot{\boldsymbol{q}}_r + \boldsymbol{C}(\boldsymbol{q}_r, \dot{\boldsymbol{q}}_r)\dot{\boldsymbol{q}}_r) + \boldsymbol{\lambda}_2\boldsymbol{G}(\boldsymbol{q}_r) = \boldsymbol{R}\boldsymbol{\tau}_v + \boldsymbol{T}_d(\boldsymbol{q}, \dot{\boldsymbol{q}}, \ddot{\boldsymbol{q}}). \tag{48}$$

By substituting (35) into (48), we obtain:

$$\begin{aligned}
&(\boldsymbol{\lambda}_1\boldsymbol{M}(\boldsymbol{q}_r) + \Delta\boldsymbol{M}(\boldsymbol{q}_r))\ddot{\boldsymbol{q}}_r + (\boldsymbol{\lambda}_1\boldsymbol{C}(\boldsymbol{q}_r, \dot{\boldsymbol{q}}_r) \\
&+ \Delta\boldsymbol{C}(\boldsymbol{q}_r, \dot{\boldsymbol{q}}_r))\dot{\boldsymbol{q}}_r) + \boldsymbol{\lambda}_2\boldsymbol{G}(\boldsymbol{q}_r) + \Delta\boldsymbol{G}(\boldsymbol{q}_r) = \boldsymbol{R}\boldsymbol{\tau}_v.
\end{aligned} \tag{49}$$

Obviously $\boldsymbol{q_r} - \boldsymbol{q}_{r0}$ is an equilibrium of system (49). Choose the Lyapunov candidate function as:

$$\begin{aligned}
V = \frac{1}{2}\dot{\boldsymbol{q}}_r^T(\boldsymbol{\lambda}_1\boldsymbol{M}(\boldsymbol{q}_r) + \Delta\boldsymbol{M}(\boldsymbol{q}_r))\dot{\boldsymbol{q}}_r + (\boldsymbol{\lambda}_2 - \boldsymbol{I})P_E(\boldsymbol{q}_r) \\
+ P_E^*(\boldsymbol{q}_r) + P_V(\boldsymbol{q}_r).
\end{aligned} \tag{50}$$

Then we have:

$$\begin{aligned}
\dot{V} =\ & \dot{\boldsymbol{q}}_r^T(\boldsymbol{\lambda}_1\boldsymbol{M}(\boldsymbol{q}_r) + \Delta\boldsymbol{M}(\boldsymbol{q}_r))\ddot{\boldsymbol{q}}_r \\
& + \frac{1}{2}\dot{\boldsymbol{q}}_r^T(\boldsymbol{\lambda}_1\dot{\boldsymbol{M}}(\boldsymbol{q}_r) + \Delta\dot{\boldsymbol{M}}(\boldsymbol{q}_r))\dot{\boldsymbol{q}}_r \\
& + \frac{d}{dt}[(\boldsymbol{\lambda}_2 - \boldsymbol{I})P_E(\boldsymbol{q}_r) + P_E^*(\boldsymbol{q}_r) + P_V(\boldsymbol{q}_r)] \\
=\ & -\dot{\boldsymbol{q}}_r^T[(\boldsymbol{\lambda}_1\boldsymbol{C}(\boldsymbol{q}_r, \dot{\boldsymbol{q}}_r) + \Delta\boldsymbol{C}(\boldsymbol{q}_r, \dot{\boldsymbol{q}}_r))\dot{\boldsymbol{q}}_r + \boldsymbol{\lambda}_2\boldsymbol{G}(\boldsymbol{q}_r) \\
& + \Delta\boldsymbol{G}(\boldsymbol{q}_r) - \boldsymbol{R}\boldsymbol{\tau}_v] + \frac{1}{2}\dot{\boldsymbol{q}}_r^T(\boldsymbol{\lambda}_1\dot{\boldsymbol{M}}(\boldsymbol{q}_r) + \Delta\dot{\boldsymbol{M}}(\boldsymbol{q}_r))\dot{\boldsymbol{q}}_r \\
& + [(\boldsymbol{\lambda}_2 - \boldsymbol{I})\frac{\partial P_E(\boldsymbol{q}_r)}{dt} + \frac{\partial P_E^*(\boldsymbol{q}_r)}{dt} + \frac{\partial P_V(\boldsymbol{q}_r)}{dt}] \\
=\ & \dot{\boldsymbol{q}}_r^T[\frac{1}{2}(\boldsymbol{\lambda}_1\dot{\boldsymbol{M}}(\boldsymbol{q}_r) + \Delta\dot{\boldsymbol{M}}(\boldsymbol{q}_r)) - (\boldsymbol{\lambda}_1\boldsymbol{C}(\boldsymbol{q}_r, \dot{\boldsymbol{q}}_r) \\
& + \Delta\boldsymbol{C}(\boldsymbol{q}_r, \dot{\boldsymbol{q}}_r))]\dot{\boldsymbol{q}}_r - \dot{\boldsymbol{q}}_r^T[\boldsymbol{\lambda}_2\boldsymbol{G}(\boldsymbol{q}_r) + \Delta\boldsymbol{G}(\boldsymbol{q}_r) - \boldsymbol{R}\boldsymbol{\tau}_v] \\
& + [(\boldsymbol{\lambda}_2 - \boldsymbol{I})\dot{\boldsymbol{q}}_r^T\boldsymbol{G}(\boldsymbol{q}_r) + \dot{\boldsymbol{q}}_r^T\boldsymbol{G}^*(\boldsymbol{q}_r) + \dot{\boldsymbol{q}}_r^T\boldsymbol{R}\boldsymbol{\tau}(\boldsymbol{q}_r)] \\
=\ & \dot{\boldsymbol{q}}_r^T[\boldsymbol{\lambda}_1(\frac{1}{2}\dot{\boldsymbol{M}}(\boldsymbol{q}_r) - \boldsymbol{C}(\boldsymbol{q}_r, \dot{\boldsymbol{q}}_r)) + \frac{1}{2}\Delta\dot{\boldsymbol{M}}(\boldsymbol{q}_r) \\
& - \Delta\boldsymbol{C}(\boldsymbol{q}_r, \dot{\boldsymbol{q}}_r)]\dot{\boldsymbol{q}}_r - \dot{\boldsymbol{q}}_r^T[\boldsymbol{G}(\boldsymbol{q}_r) + \Delta\boldsymbol{G}(\boldsymbol{q}_r)] + \dot{\boldsymbol{q}}_r^T\boldsymbol{G}^*(\boldsymbol{q}_r) \\
\leq\ & 0.
\end{aligned}$$

Therefore, we can conclude that the equilibrium is stable. This completes the proof.

APPENDIX D
SYSTEM IDENTIFICATION

The proposed identification method [33] is designed based on a constrained QP problem expressed as follows:

$$\begin{aligned}
\text{Find } \boldsymbol{\Phi}^* \in \ & \min_{\boldsymbol{\Phi}} \| \bar{\mathbf{F}} - \bar{\mathbf{W}}\boldsymbol{\Phi} \|_2^2 + \| \boldsymbol{\Phi}_{CAD} - \boldsymbol{\Phi} \|_2^2 \\
\text{subject to} \quad & \\
& M_i \geq 0 \\
& CoM_i^- \leq CoM_i \leq CoM_i^+ \\
& I_i > 0 \\
& \boldsymbol{\Phi}_b^* = \Psi(\mathbf{M}_n, \mathbf{MX}_n, \mathbf{I}_{\mathbf{z}n})
\end{aligned} \tag{51}$$

where $\boldsymbol{\Phi}_{CAD}$ ($(3 \times 6) \times 1$) refers to the inertial parameters values obtained from the CAD of the exoskeleton and the anthropometric table [48], and $\boldsymbol{\Phi}_b^*$ ($(3\times6)\times1$) to the estimated ones. CoM_i^- and CoM_i^+ are upper and lower bounds of CoM position along the i^{th} link. Ψ expresses the constraints between the BP and inertial parameters. $\mathbf{M}_n \in R^{6\times1}$ is the mass vector, $\mathbf{MX}_n \in R^{6\times1}$ is vector of the first moment of inertia along the link, and $\mathbf{I}_{\mathbf{z}n} \in R^{6\times1}$ is the vector of the segment inertia. n denotes the number of links (n=6).

This constrained QP performs the least-square fitting of measured external force and moment while minimizing the deviation between the estimated inertial parameters and their CAD/anthropomorphic values. Using the set of four constraints, physical consistencies of inertial parameters are guaranteed.

REFERENCES

[1] P. Dehail, E. Bestaven, F. Muller, A. Mallet, B. Robert, I. Bourdel-Marchasson, and J. Petit, "Kinematic and electromyographic analysis of rising from a chair during a "sit-to-walk" task in elderly subjects: role of strength," *Clinical Biomechanics*, vol. 22, no. 10, pp. 1096–1103, 2007.

[2] M. Galli, V. Cimolin, M. Crivellini, and I. Campanini, "Quantitative analysis of sit to stand movement: experimental set-up definition and application to healthy and hemiplegic adults," *Gait & Posture*, vol. 28, no. 1, pp. 80–85, 2008.

[3] P. O. Riley, D. E. Krebs, R. Popat *et al.*, "Biomechanical analysis of failed sit-to-stand," *IEEE Transactions on Rehabilitation Engineering*, vol. 5, no. 4, pp. 353–359, 1997.

[4] S. H. Smith, P. Reilly, and A. M. Bull, "A musculoskeletal modelling approach to explain sit-to-stand difficulties in older people due to changes in muscle recruitment and movement strategies," *Journal of Biomechanics*, vol. 98, pp. 109–451, 2020.

[5] M. A. Hughes, B. S. Myers, and M. L. Schenkman, "The role of strength in rising from a chair in the functionally impaired elderly," *Journal of Biomechanics*, vol. 29, no. 12, pp. 1509–1513, 1996.

[6] Y. R. Mao, X. Q. Wu, J. L. Zhao, W. L. A. Lo, L. Chen, M. H. Ding, Z. Q. Xu, R. H. Bian, D. F. Huang, and L. Li, "The crucial changes of sit-to-stand phases in subacute stroke survivors identified by movement decomposition analysis," *Frontiers in Neurology*, vol. 9, p. 185, 2018.

[7] A. Boukadida, F. Piotte, P. Dehail, and S. Nadeau, "Determinants of sit-to-stand tasks in individuals with hemiparesis post stroke: a review," *Annals of physical and rehabilitation medicine*, vol. 58, no. 3, pp. 167–172, 2015.

[8] A. M. Dollar and H. Herr, "Lower extremity exoskeletons and active orthoses: challenges and state-of-the-art," *IEEE Transactions on Robotics*, vol. 24, no. 1, pp. 144–158, 2008.

[9] W. Huo, S. Mohammed, J. C. Moreno, and Y. Amirat, "Lower limb wearable robots for assistance and rehabilitation: A state of the art," *IEEE Systems Journal*, vol. 10, no. 3, pp. 1068–1081, 2016.

[10] A. J. Young and D. P. Ferris, "State of the art and future directions for lower limb robotic exoskeletons," *IEEE Transactions on Neural Systems and Rehabilitation Engineering*, vol. 25, no. 2, pp. 171–182, 2016.

[11] S. Mefoued, S. Mohammed, Y. Amirat, and G. Fried, "Sit-to-stand movement assistance using an actuated knee joint orthosis," in *2012 4th IEEE RAS & EMBS International Conference on Biomedical Robotics and Biomechatronics (BioRob)*, 2012, pp. 1753–1758.

[12] A. Tsukahara, R. Kawanishi, Y. Hasegawa, and Y. Sankai, "Sit-to-stand and stand-to-sit transfer support for complete paraplegic patients with robot suit hal," *Advanced robotics*, vol. 24, no. 11, pp. 1615–1638, 2010.

[13] D. F. P. Granados, H. Kadone, and K. Suzuki, "Unpowered lower-body exoskeleton with torso lifting mechanism for supporting sit-to-stand transitions," in *2018 IEEE/RSJ International Conference on Intelligent Robots and Systems (IROS)*, 2018, pp. 2755–2761.

[14] N. Karavas, A. Ajoudani, N. Tsagarakis, J. Saglia, A. Bicchi, and D. Caldwell, "Tele-impedance based stiffness and motion augmentation for a knee exoskeleton device," in *IEEE International Conference on Robotics and Automation (ICRA)*, 2013, pp. 2194–2200.

[15] J. Vantilt, K. Tanghe, M. Afschrift, A. K. Bruijnes, K. Junius, J. Geeroms, E. Aertbeliën, F. De Groote, D. Lefeber, I. Jonkers *et al.*, "Model-based control for exoskeletons with series elastic actuators evaluated on sit-to-stand movements," *Journal of Neuroengineering and Rehabilitation*, vol. 16, no. 1, pp. 1–21, 2019.

[16] Z. Matjačić, M. Zadravec, and J. Oblak, "Sit-to-stand trainer: an apparatus for training "normal-like" sit to stand movement," *IEEE Transactions on Neural Systems and Rehabilitation Engineering*, vol. 24, no. 6, pp. 639–649, 2015.

[17] O. N. Aroche, P.-J. Meyer, S. Tu, A. Packard, and M. Arcak, "Robust control of the sit-to-stand movement for a powered lower limb orthosis," *IEEE Transactions on Control Systems Technology*, 2019.

[18] X. Liu, Z. Zhou, J. Mai, and Q. Wang, "Real-time mode recognition based assistive torque control of bionic knee exoskeleton for sit-to-stand and stand-to-sit transitions," *Robotics and Autonomous Systems*, vol. 119, pp. 209–220, 2019.

[19] C. Fleischer and G. Hommel, "A human–exoskeleton interface utilizing electromyography," *IEEE Transactions on Robotics*, vol. 24, no. 4, pp. 872–882, 2008.

[20] G. Aguirre-Ollinger, J. E. Colgate, M. A. Peshkin, and A. Goswami, "Active-impedance control of a lower-limb assistive exoskeleton," in *IEEE International Conference on Rehabilitation Robotics*, 2007, pp. 188–195.

[21] V. Rajasekaran, M. Vinagre, and J. Aranda, "Event-based control for sit-to-stand transition using a wearable exoskeleton," in *2017 International Conference on Rehabilitation Robotics (ICORR)*, 2017, pp. 400–405.

[22] K. Tanghe, A. Harutyunyan, E. Aertbeliën, F. De Groote, J. De Schutter, P. Vrancx, and A. Nowé, "Predicting seat-off and detecting start-of-assistance events for assisting sit-to-stand with an exoskeleton," *IEEE Robotics and Automation Letters*, vol. 1, no. 2, pp. 792–799, 2016.

[23] W. Hassani, S. Mohammed, and Y. Amirat, "Real-time emg driven lower limb actuated orthosis for assistance as needed movement strategy." in *Robotics: Science and Systems (RSS)*, 2013.

[24] S. Oh, K. Kong, and Y. Hori, "Design and analysis of force-sensorless power-assist control," *IEEE Transactions on Industrial Electronics*, vol. 61, no. 2, pp. 985–993, 2014.

[25] L. Liu, Z. Hong, B. Penzlin, B. Misgeld, C. Ngo, L. Bergmann, and S. Leonhardt, "Low impedance-guaranteed gain-scheduled geso for torque-controlled vsa, with application of exoskeleton-assisted sit-to-stand," *IEEE/ASME Transactions on Mechatronics*, 2020.

[26] S. R. Lord, S. M. Murray, K. Chapman, B. Munro, and A. Tiedemann, "Sit-to-stand performance depends on sensation, speed, balance, and psychological status in addition to strength in older people," *The Journals of Gerontology Series A: Biological Sciences and Medical Sciences*, vol. 57, no. 8, pp. M539–M543, 2002.

[27] T. Yan, M. Cempini, C. M. Oddo, and N. Vitiello, "Review of assistive strategies in powered lower-limb orthoses and exoskeletons," *Robotics and Autonomous Systems*, vol. 64, pp. 120–136, 2015.

[28] D. Pinto-Fernandez, D. Torricelli, M. del Carmen Sanchez-Villamanan, F. Aller, K. Mombaur, R. Conti, N. Vitiello, J. C. Moreno, and J. L. Pons, "Performance evaluation of lower limb exoskeletons: a systematic review," *IEEE Transactions on Neural Systems and Rehabilitation Engineering*, vol. 28, no. 7, pp. 1573–1583, 2020.

[29] E. Papa and A. Cappozzo, "Sit-to-stand motor strategies investigated in able-bodied young and elderly subjects," *Journal of Biomechanics*, vol. 33, no. 9, pp. 1113–1122, 2000.

[30] A. Mohammadi, M. Tavakoli, H. Marquez, and F. Hashemzadeh, "Nonlinear disturbance observer design for robotic manipulators," *Control Engineering Practice*, vol. 21, no. 3, pp. 253–267, 2013.

[31] W. Huo, S. Mohammed, and Y. Amirat, "Impedance reduction control of a knee joint human-exoskeleton system," *IEEE Transactions on Control Systems Technology*, vol. 27, no. 6, pp. 2541–2556, 2018.

[32] W. Huo, S. Mohammed, Y. Amirat, and K. Kong, "Active impedance control of a lower limb exoskeleton to assist sit-to-stand movement," in *IEEE International Conference on Robotics and Automation*, 2016, pp. 3530–3536.

[33] V. Bonnet and G. Venture, "Fast determination of the planar body segment inertial parameters using affordable sensors," *IEEE Transactions on Neural Systems and Rehabilitation Engineering*, vol. 23, no. 4, pp. 628–635, 2015.

[34] M. Grün and U. Konigorski, "Observer based method for joint torque estimation in active orthoses," in *Mathematical Modelling*, vol. 7, no. 1, 2012, pp. 199–204.

[35] J. J. Craig, *Introduction to robotics: mechanics and control*. Pearson Prentice Hall Upper Saddle River, 2005.

[36] F. F. Russell, P. Kormushev, R. Vaidyanathan, and P. Ellison, "The impact of acl laxity on a bicondylar robotic knee and implications in human joint biomechanics," *IEEE Transactions on Biomedical Engineering*, 2020.

[37] M. K. Mak, O. Levin, J. Mizrahi, and C. W. Hui-Chan, "Joint torques during sit-to-stand in healthy subjects and people with parkinson's disease," *Clinical Biomechanics*, vol. 18, no. 3, pp. 197–206, 2003.

[38] S. Buatois, D. Miljkovic, P. Manckoundia, R. Gueguen, P. Miget, G. Vançon, P. Perrin, and A. Benetos, "Five times sit to stand test is a predictor of recurrent falls in healthy community-living subjects aged 65 and older," *Journal of the American Geriatrics Society*, vol. 56, no. 8, pp. 1575–1577, 2008.

[39] W.-H. Chen, "Disturbance observer based control for nonlinear systems," *IEEE/ASME Transactions on Mechatronics*, vol. 9, no. 4, pp. 706–710, 2004.

[40] L. Liu, S. Leonhardt, C. Ngo, and B. J. Misgeld, "Impedance-controlled variable stiffness actuator for lower limb robot applications," *IEEE Transactions on Automation Science and Engineering*, vol. 17, no. 2, pp. 991–1004, 2019.

[41] R. Mallat, V. Bonnet, W. Huo, P. Karasinski, Y. Amirat, M. Khalil, and S. Mohammed, "Human-exoskeleton system dynamics identification using affordable sensors," in *2018 IEEE International Conference on Robotics and Automation (ICRA)*, 2018, pp. 6759–6765.

[42] W. Khalil and E. Dombre, *Modeling, identification and control of robots*. Butterworth-Heinemann, 2004.

[43] M. Gautier, "Numerical calculation of the base inertial parameters of robots," *Journal of robotic systems*, vol. 8, no. 4, pp. 485–506, 1991.
[44] J. Jovic, A. Escande, K. Ayusawa, E. Yoshida, A. Kheddar, and G. Venture, "Humanoid and human inertia parameter identification using hierarchical optimization," *IEEE Transactions on Robotics*, vol. 32, no. 3, pp. 726–735, 2016.
[45] W. Huo, M. A. Alouane, Y. Amirat, and S. Mohammed, "Force control of sea-based exoskeletons for multimode human–robot interactions," *IEEE Transactions on Robotics*, vol. 36, no. 2, pp. 570–577, 2008.
[46] S. Oh, E. Baek, S.-k. Song, S. Mohammed, D. Jeon, and K. Kong, "A generalized control framework of assistive controllers and its application to lower limb exoskeletons," *Robotics and Autonomous Systems*, vol. 73, pp. 68–77, 2015.
[47] K. Kong and M. Tomizuka, "A gait monitoring system based on air pressure sensors embedded in a shoe," *IEEE/ASME Transactions on mechatronics*, vol. 14, no. 3, pp. 358–370, 2009.
[48] P. De Leva, "Adjustments to Zatsiorsky-Seluyanov's segment inertia parameters," *Journal of Biomechanics*, vol. 29, no. 9, pp. 1223–1230, 1996.
[49] C. Yang, G. Ganesh, S. Haddadin, S. Parusel, A. Albu-Schaeffer, and E. Burdet, "Human-like adaptation of force and impedance in stable and unstable interactions," *IEEE transactions on Robotics*, vol. 27, no. 5, pp. 918–930, 2011.
[50] K. Kong and M. Tomizuka, "Control of exoskeletons inspired by fictitious gain in human model," *IEEE/ASME Transactions on Mechatronics*, vol. 14, no. 6, pp. 689–698, 2009.
[51] E. Burdet, R. Osu, D. W. Franklin, T. E. Milner, and M. Kawato, "The central nervous system stabilizes unstable dynamics by learning optimal impedance," *Nature*, vol. 414, no. 6862, pp. 446–449, 2001.
[52] M. Cifrek, V. Medved, S. Tonković, and S. Ostojić, "Surface emg based muscle fatigue evaluation in biomechanics," *Clinical Biomechanics*, vol. 24, no. 4, pp. 327–340, 2009.



Weiguang Huo received the B.S. degree in measurement and control technology and instruments from the Wuhan University of Technology, Wuhan, China, in 2009, the M.S. degree in control theory and control engineering from the Huazhong University of Science and Technology, Wuhan, in 2012, and the Ph.D. degree in signal, image and automation from the University of Paris-Est, Créteil, France, in 2016. He is currently a Research Associate at Imperial College London. His current research interests include modeling and control of wearable robotic systems and functional electrical stimulation.



Huiseok Moon received the B.S. degree in the division of robotics from Kwangwoon University, Seoul, South Korea in 2017, and the M.S. degree in mechanical engineering from Sogang University, Seoul, South Korea in 2019, respectively. In 2019, he joined LISSI, UPEC, Vitry-sur-seine, France, where he is currently a candidate of Ph.D. His current research interests include modelling and control of human-robot physical interaction systems also known as wearable robots.



Mohamed Amine Alouane received the engineering and the Master of Science (MSc) degrees both from the Ecole Militaire Polytechnique (EMP), Bordj-el-Bahri, Algiers, Algeria (in 2016). He received Ph.D. degree in Automatic and Robotics from Paris Est University in 2020. He is currently an assistant professor at the EMP and a member in the laboratory of Complex Systems Control Simulation (CSCS). His research interests include nonlinear robust control, modeling and control of wearable robotic systems as well as functional electrical stimulation.



Vincent Bonnet received the MsC. degree and the Ph.D. degree in automatics control and robotics, from the Science University of Montpellier 2. In 2010 he was a post-doc at the University of Rome Foro Italico, Italy. In 2014 he became a post-doc for the Japanese Society for Promotion of Research at the Tokyo University of Agriculture and Technology Tokyo, Japan. Since 2016 he is associate professor at the University of Paris-Est Créteil. His research interests are very interdisciplinary and include low-cost sensors, humanoid robotics, system identification motion analysis, and control.



Jian Huang (Senior Member, IEEE) received the graduate, master of engineering, and Ph.D. degrees from the Huazhong University of Science and Technology (HUST), Wuhan, China, in 1997, 2000, and 2005, respectively. From 2006 to 2008, he was a Postdoctoral Researcher with the Department of Micro-Nano System Engineering and the Department of Mechano-Informatics and Systems, Nagoya University, Nagoya, Japan. He is currently a Full Professor with the School of Artificial Intelligence and Automation, HUST. His main research interests include rehabilitation robots, robotic assembly, networked control systems, and bioinformatics.



Yacine Amirat received the Ph.D. degree in robotics from the University of Pierre et Marie Curie, Paris, France, in 1989, and the Habilitation degree in artificial intelligence and control of robotic systems from the University of Paris 12-France, Paris, in 1996. He is currently the Director of the Laboratory of Image, Signal and Intelligent Systems (LISSI) UPEC, and the Scientific Director of several research projects. He has authored or co-authored more than 180 papers in scientific journals, books, and conference proceedings. His research interests include intelligent robots and systems, assistive robotics, wearable robots, cognitive robotics and ambient intelligence. Prof. Amirat is regularly involved in conference and workshop organization committees. He is also involved in editorial activities of several IEEE-RAS conferences and journals (ICRA, IROS, RA-L, T-ASE). He is actively collaborating with industrial and academic partners in various European projects.



Ravi Vaidyanathan is a Reader at Imperial College London, His laboratory (Biomechatroics Laboratory: http://www.biomechatronicslab.co.uk/) focuses on optimisation and learning algorithms for sensor fusion in smart systems, with applications ranging from human performance, smart environments, and robotics. Dr Vaidyanathan's research has resulted in 200+ refereed publications, 6 pending patents and has been featured for impact by: the RAEng, BBC, New Scientist, The Engineer, Inc. Magazine, IEEE Institute, Flight Global Magazine, The Times of India, The Discovery Channel, and the Tokyo Broadcasting Company. The Biomechatroncis Laboraotory has supported the formation of 4 new companies that have introduced 3 new commercial products in smart systems in the last 5 years alone. He has been invited to present his research at the US Pentagon, UK Parliament and the UK Prime Minister's Residence at 10 Downing Street. and is currently co-chair of the IEEE Robotics and Automation Society Technical Advisory Committee on Biorobotics.



Samer Mohammed (Senior Member, IEEE) received the Ph.D. degree in computer science from University of Montpellier (LIRMM/CNRS), Montpellier, France in 2006. He is currently a Full Professor with the University of Paris-Est Créteil. He has authored or co-authored over 100 papers in scientific journals, books, and conference proceedings. His current research interests include modeling, identification, and control of robotic systems (wearable robots) as well as artificial intelligence, and decision-support theory with target applications on functional assistance and rehabilitation of dependent people.